

RADIOCARBON CALIBRATION AND COMPARISON TO 50 KYR BP WITH PAIRED ^{14}C AND ^{230}Th DATING OF CORALS FROM VANUATU AND PAPUA NEW GUINEA

K B Cutler^{1,2} • S C Gray³ • G S Burr⁴ • R L Edwards¹ • F W Taylor⁵ • G Cabioch⁶ • J W Beck⁴ • H Cheng¹ • J Moore⁴

ABSTRACT. We calibrated portions of the radiocarbon time scale with combined ^{230}Th , ^{231}Pa , ^{14}C measurements of corals collected from Espiritu Santo, Vanuatu and the Huon Peninsula, Papua New Guinea. The new data map ^{14}C variations ranging from the current limit of the tree-ring calibration [11,900 calendar years before present (cal BP), Kromer and Spurk 1998, now updated to 12,400 cal BP, see Kromer et al., this issue], to the ^{14}C -dating limit of 50,000 cal BP, with detailed structure between 14 to 16 cal kyr BP and 19 to 24 cal kyr BP. Samples older than 25,000 cal BP were analyzed with high-precision ^{231}Pa dating methods (Pickett et al. 1994; Edwards et al. 1997) as a rigorous second check on the accuracy of the ^{230}Th ages. These are the first coral calibration data to receive this additional check, adding confidence to the age data forming the older portion of the calibration. Our results, in general, show that the offset between calibrated and ^{14}C ages generally increases with age until about 28,000 cal BP, when the recorded ^{14}C age is nearly 6800 yr too young. The gap between ages before this time is less; at 50,000 cal BP, the recorded ^{14}C age is 4600 yr too young. Two major ^{14}C -age plateaus result from a 130‰ drop in $\Delta^{14}\text{C}$ between 14–15 cal kyr BP and a 700‰ drop in $\Delta^{14}\text{C}$ between 22–25 cal kyr BP. In addition, a large atmospheric $\Delta^{14}\text{C}$ excursion to values over 1000‰ occurs at 28 cal kyr BP. Between 20 and 10 cal kyr BP, a component of atmospheric $\Delta^{14}\text{C}$ anti-correlates with Greenland ice $\delta^{18}\text{O}$, indicating that some portion of the variability in atmospheric $\Delta^{14}\text{C}$ is related to climate change, most likely through climate-related changes in the carbon cycle. Furthermore, the 28-kyr excursion occurs at about the time of significant climate shifts. Taken as a whole, our data indicate that in addition to a terrestrial magnetic field, factors related to climate change have affected the history of atmospheric ^{14}C .

INTRODUCTION

The radiocarbon dating method has been widely applied since its development in the 1950s (Libby 1955). Its time range from about 50,000 yr ago to the present, applicability to a wide variety of materials, and high-precision age determinations make it the predominant means of age control for the end of the Quaternary period. The ^{14}C age equation, however, is based on the assumption of constant atmospheric $^{14}\text{C}/^{12}\text{C}$. Changes in atmospheric $^{14}\text{C}/^{12}\text{C}$ ($\Delta^{14}\text{C}$) over time are well documented and are attributed to changes in the earth's magnetic field, variability in solar activity, and shifts in the rates of exchange within the global carbon cycle (Suess 1970). The first two controls modulate the ^{14}C production rate, while the third governs the distribution of ^{14}C among the earth's carbon reservoirs after it is produced. For these reasons, ^{14}C ages require calibration with an independent chronometer.

Over the last half-century, intensive efforts have been devoted to calibrating the ^{14}C time scale. An accurate and precise ^{14}C calibration allows the true age of a sample to be established from the ^{14}C age, which is essential for comparing ^{14}C -dated records with records dated by other means, and for establishing rates of change. The calibration also furnishes the history of atmospheric $\Delta^{14}\text{C}$. This history contains important clues about past changes in the global climate system linked to shifts in carbon cycling.

Tree-ring counts provide a continuous and high-resolution (bidecadal) calibration from present day back to 11,855 ± 20 cal BP (calendar years before present, 0 BP = AD 1950) (Kromer and Spurk

¹Minnesota Isotope Laboratory, Department of Geology and Geophysics, University of Minnesota, 310 Pillsbury Drive, SE, Minneapolis, Minnesota 55455, USA.

²Corresponding author. Email: drscutler@earthlink.net.

³Marine and Environmental Studies, University of San Diego, Alcalá Park, San Diego, California 92110, USA.

⁴NSF-Arizona AMS Laboratory, University of Arizona, Physics Department, Tucson, Arizona 85721, USA.

⁵Institute for Geophysics, University of Texas, 4412 Spicewood Springs Road, Bld. 600, Austin, Texas 78759-8500, USA.

⁶Institut de Recherche pour le Développement (IRD), BPA5, Nouméa, New Caledonia.

1998). (This has now been extended to 12,400 cal BP; see Kromer et al., this issue.) However, extending the dendrocalibration back in time has become difficult due to the scarcity of appropriate fossil tree specimens. As a result, a number of studies have explored the suitability of other chronometers in calibrating older portions of the ^{14}C time scale.

With the development of high-precision ^{230}Th dating techniques in the late 1980s (Edwards et al. 1987a,b, 1988; Edwards 1988), fossil corals have become a prominent calibration tool. The use of ^{230}Th for high-resolution ^{14}C calibrations was first proposed and tested by Edwards et al. (1988). Despite this possibility, obtaining sequences of corals for the period needed in the calibration was a significant challenge because these corals are submerged well below present sea level. In 1989, Fairbanks was able to recover corals that grew since the Last Glacial Maximum (LGM) through underwater drilling off the coast of Barbados. A field expedition to Papua New Guinea in 1988 headed by Bloom and Chappell was also successful in obtaining the last half of the deglacial sequence by drilling into uplifted shorelines.

These methods for recovering late-Quaternary coral samples were further developed in subsequent studies, and, through the use of high-precision, paired ^{230}Th - ^{14}C dating of the corals, individual points (Bard et al. 1990, 1993, 1996, 1998; Edwards et al. 1993) or high-resolution sequences (Burr et al. 1998) have been added to the calibration curve with as little as 3‰ error in the ^{230}Th age. Each calibration point in the former case is established from a single coral colony. In the latter case, a sequence of points are established through combined ^{14}C dating and counting of annual growth bands in a single coral head; the results, averaged over 10 yr to achieve decadal resolution, are then located on the calibration curve using the coral's ^{230}Th age range. To address the possibility of diagenetically-altered ^{230}Th ages, procedures were developed early on (Edwards et al. 1993; Gallup et al. 1994) for identifying altered samples through the comparison of the coral's initial $^{234}\text{U}/^{238}\text{U}$ ratio ($\delta^{234}\text{U}_i$) with the modern marine $\delta^{234}\text{U}$ value.

If we consider the cumulative coral calibration data, analyzed with high-precision ^{230}Th methods (Bard et al. 1990, 1993, 1996, 1998; Edwards et al. 1993; Burr et al. 1998) and screened based on a comparison between its measured uranium isotopic value and the known modern marine value (see Methods section), the following picture emerges. The interval between 11.9 and 14 cal kyr BP consists of about 20 points and a high-resolution sequence between 11.7 and 12.4 cal kyr BP. The 10-kyr interval between 14 and 24 cal kyr BP, however, is represented by only 8 points. Beyond 24 cal kyr BP, there is a solitary point at 30.2 cal kyr BP. In general, the gap between the calibrated and ^{14}C ages increases with age: at 12 cal kyr BP, the ^{14}C age is about 1700 yr too young, and at 30 cal kyr BP, the ^{14}C age is about 4000 yr too young. The low resolution in the older time range is due to the inherent difficulty in retrieving well-preserved samples of the appropriate age.

In addition to coral calibration methods, other techniques have been employed to extend the calibration beyond the range of tree rings. One method developed in the 1970s (Tauber 1970) uses seasonally laminated sediments as an annual clock for ^{14}C -dated materials contained within the laminae, such as plant macrofossils and foraminifera. Recent use of this method on laminated lake sediments (Kitagawa and van der Plicht 1998; Goslar et al. 1995, 2000; Hajdas et al. 1993, 1995) and marine sediments (Hughen et al. 1998, 2000) has produced continuous calibration curves, some of which extend to 45,000 yr, near the limit of the ^{14}C time scale. Other methods that show promise include ^{230}Th dating of stalagmites (Vogel and Kronfeld 1998; Genty et al. 1999; Beck et al. 2001), ^{234}U - ^{230}Th isochron dating of aragonite and lignite (Schramm et al. 2000; Geyh and Schluchter 1998), application of other dating methods (Stuiver 1978), and correlation of ^{14}C -dated deep-sea records with the GISP2 Greenland ice-core chronology (Voelker et al. 1998; van Kreveld et al. 2000;

Bard et al. 2004; Hughen et al. 2004). Stuiver et al. (1998) created a curve that can be used for ¹⁴C calibration (IntCal98) which is based on records derived from tree rings (0 to 11.9 cal kyr BP; Kromer and Spurk 1998), laminated marine sediments (11.9 to 14.5 cal kyr BP; Hughen et al. 1998), and corals (11.9 to 24 cal kyr BP; Bard et al. 1990, 1993, 1996, 1998; Edwards et al. 1993; Burr et al. 1998) and extends to 24 cal kyr BP. The combined records provide detailed structure between 14 cal kyr BP and present. However, prior to 14 cal kyr BP, questions related to resolution or accuracy of the record remain.

In this study, we analyze over 70 corals using high-precision ¹⁴C and ²³⁰Th dating techniques to improve the resolution of portions of the calibration and to extend it beyond its current limit. To do this, we followed the strategy of drilling into uplifted shorelines to obtain deglacial and earlier corals and collected drill core samples at sites in Vanuatu and Papua New Guinea. This strategy allowed us to recover some unique samples as well as sequences of samples of higher resolution than earlier studies. Because older corals are more likely to have undergone diagenesis, we applied parameters, in addition to δ²³⁴U_i values, to detect alteration in corals more than 25 kyr old. High-resolution ²³¹Pa dating methods (Pickett et al. 1994; Edwards et al. 1997) provided a rigorous second check on the accuracy of ²³⁰Th ages and add confidence to those portions of the calibration established from samples that record concordant ²³⁰Th and ²³¹Pa ages. This is the first coral calibration study to employ such methods.

FIELD AREA AND SAMPLING METHODS

The field area consists of 6 sites (Figures 1 and 2). Tasmaloum and Urelapa are located at the southern tip of Espiritu Santo, Vanuatu and have uplift rates of roughly 4.6 m/kyr and 3.4 m/kyr, respectively. Kwambu, Kanzarua, Kanomi, and Gagidu Point are located on the Huon Peninsula in northeastern Papua New Guinea and have uplift rates of 1.9 m/kyr (Stein et al. 1993), 2.8 m/kyr (Ota et al. 1993), 2.6 m/kyr and 2.1 m/kyr, respectively (Cutler et al. 2003).

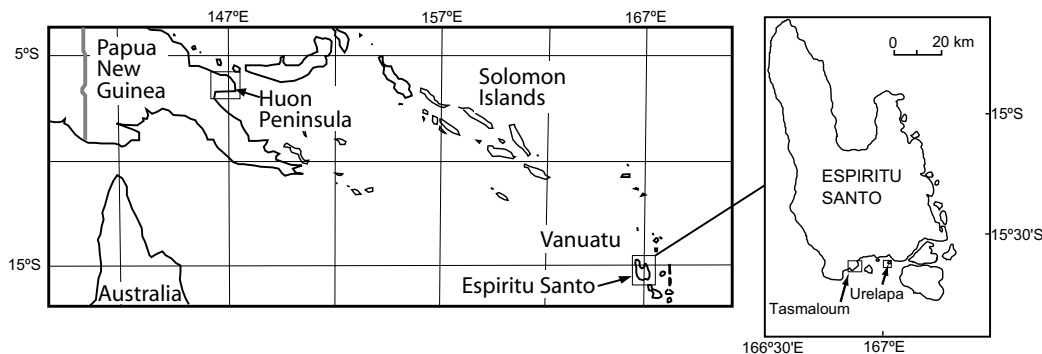


Figure 1 Maps of field areas. Boxes show areas depicted in Figure 2.

Coral samples were drilled from Tasmaloum, Urelapa, Kwambu, Kanomi, and Gagidu Point during 6 drilling operations that took place between 1988–1997. A total of 20 drill cores, 17 from Vanuatu and 3 from Papua New Guinea, are used in the study (Figures 2 and 3, Appendix). All cores were retrieved onshore and all were drilled vertically except Vanuatu cores 9H, 9J, 9L, 12, 14, which were drilled at angles of 20 to 30° (Figure 3, Appendix) to recover offshore samples. Rapidly uplifting coastlines were selected, as in previous studies (Chappell and Polach 1991; Edwards et al. 1993; Burr et al. 1998), to reduce the drill depth required to reach older corals that grew when sea level

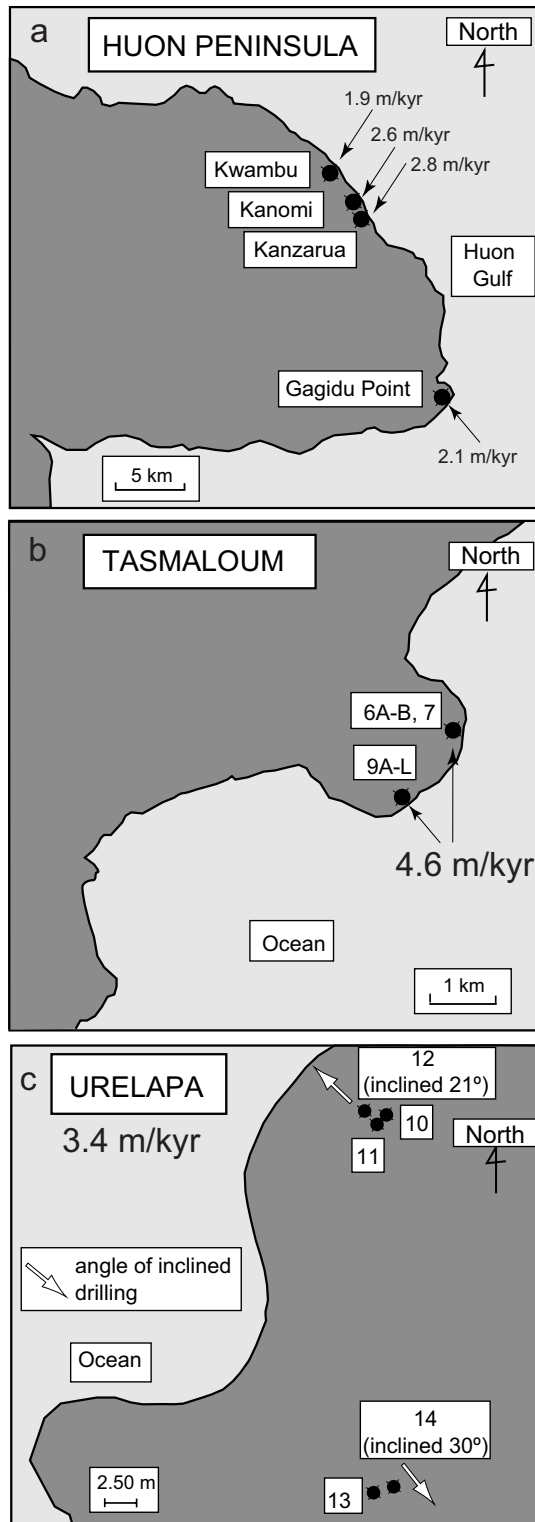


Figure 2 Plan views of sampling sites. In (a) drilling sites are at Kwambu, Kanzarua, and Gagidu Point. There is also surface collection in Kanzarua and Kwambu. Drilling sites in (b) and (c) are indicated by solid symbols. Uplift rates are indicated in (a), (b), and (c).

was well below its present level. Because of this approach, the depth required to reach Last Glacial Maximum (LGM) corals that grew about 120 m below present sea level (Fairbanks et al. 1989) is reduced by 40 to 100 m for coastlines uplifting at 2 to 5 m/kyr, respectively. Core depths range from 15 to 95 m and LGM material was recovered from 9 cores. Of the 74 samples analyzed in this study, 68 were obtained from drill cores. The remaining 6 are from surface exposures at Kwambu and Kanzarua, from 9 to 75 m above present sea level.

ANALYTICAL METHODS

As an initial screen for altered or contaminated samples, all corals were examined for visible evidence of diagenesis or recrystallization and were subjected to X-ray diffraction analyses, which indicate the presence of calcite (in excess of 1%) formed during diagenesis. Those that appeared pristine and contained no detectable calcite were included in the study.

¹⁴C Technique

All samples were subjected to a selective dissolution procedure as an additional measure to eliminate contaminated material prior to ¹⁴C isotopic analyses. Diagenetic processes can add significant amounts of carbon to corals with high ¹⁴C/¹²C ratios and potentially alter the ¹⁴C ages. Selective dissolution dissolves away the outer portion (~50%) of the skeletal structure, thereby removing such contaminants (Burr et al. 1992).

The present ¹⁴C/¹²C ratio of each sample was established using accelerator mass spectrometry (AMS) at the National Science Foundation Accelerator Facility for Radioisotope Analysis at the University of Arizona, Tucson, USA. The data reported here are given as ¹⁴C ages and $\Delta^{14}\text{C}$ values. $\Delta^{14}\text{C}$ is a measure of the deviation of the atmospheric ¹⁴C/¹²C content at a given time from the pre-industrial atmospheric value in 1850 in parts per thousand; positive values indicate an excess in ¹⁴C relative to 1850, and negative values indicate a relative deficit. $\Delta^{14}\text{C}$ is calculated from present ¹⁴C/¹²C and ²³⁰Th age and is corrected for decay of ¹⁴C over time. The analytical methods and calculation of ¹⁴C ages and $\Delta^{14}\text{C}$ values are detailed in Burr et al. (1998). The reported uncertainty in $\Delta^{14}\text{C}$ includes uncertainties in the ¹⁴C and ²³⁰Th ages (Burr et al. 1998).

Reported ¹⁴C ages were also corrected for the reservoir age of surface water at the sample site. A reservoir correction of 500 yr was used for Tasmaloum samples (Burr et al. 1998) and 400 yr for Urelapa and Papua New Guinea (Edwards et al. 1993) samples.

²³⁰Th and ²³¹Pa Techniques

Coral ²³⁰Th and ²³¹Pa ages were measured at the University of Minnesota using thermal ionization mass spectrometry (TIMS). ²³⁰Th methods are modifications of those of Edwards et al. (1987a,b, 1988), as described by Cheng et al. (2000). ²³¹Pa methods are those of Shen et al. (2003) and Edwards et al. (1997), which are modifications of those of Pickett et al. (1994). ²³⁰Th ages were screened for alteration using the initial ²³⁴U/²³⁸U ($\delta^{234}\text{U}_i$) value (Edwards et al. 1993) and, for samples older than 25 cal kyr BP, ²³⁰Th-²³¹Pa age concordancy.

During coral growth, the coral $\delta^{234}\text{U}$ value is indistinguishable from the marine value (Cheng et al. 2000). Because the coral $\delta^{234}\text{U}$ value is sensitive to isotopic exchange of uranium after skeletal growth, comparison of this value with the modern marine $\delta^{234}\text{U}$ value provides an indicator of coral diagenesis. Here, the coral $\delta^{234}\text{U}$ value is considered indistinguishable from the modern marine value when the sample $\delta^{234}\text{U}_i$ values are within $\pm 8\%$ of the modern marine value and the 2- σ analytical errors are $\leq 8\%$. The previously reported marine $\delta^{234}\text{U}$ value was 149.3‰ (Galewskyr et al.

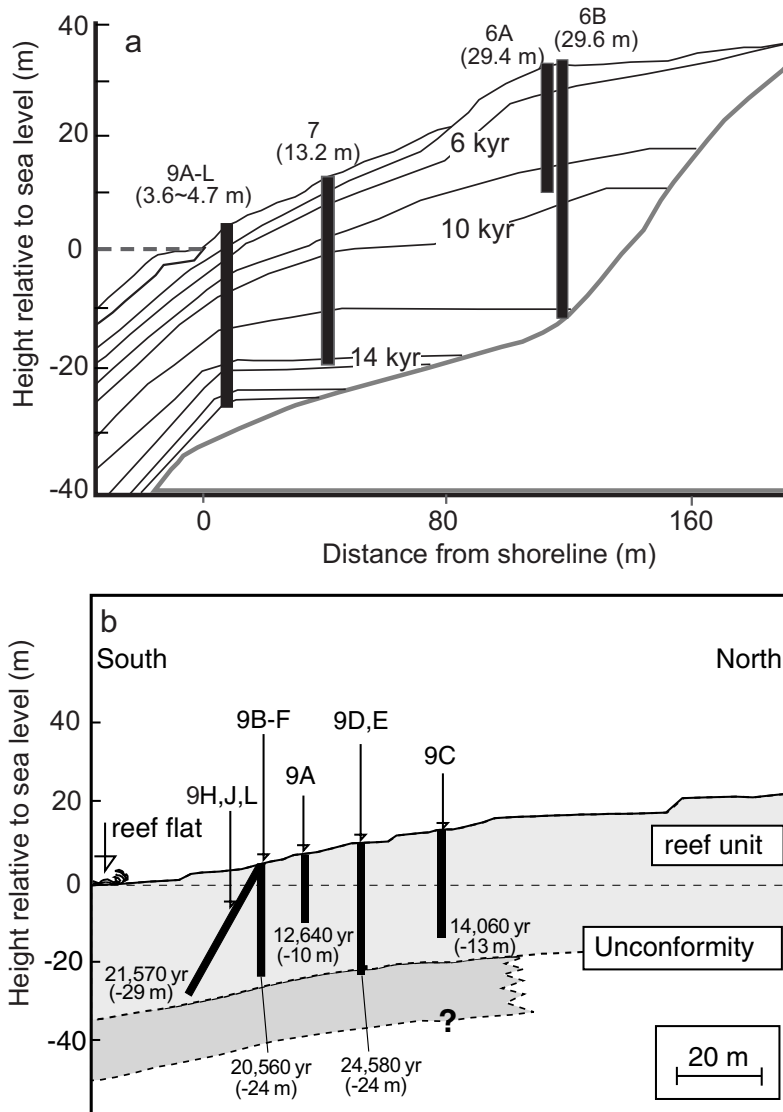


Figure 3 Cross-sections of Tasmaloum drill sites: (a) schematic cross-section perpendicular to shoreline at sites 6 and 7. For comparison, the drill holes at site 9 have been projected onto it. Contour lines, based on sample ages and depths (Table 1), are at 2-kyr age intervals and are interpolated between cores. Vertical exaggeration is 2×; (b) schematic cross-section perpendicular to shoreline at site 9. The top ages in each of these cores was roughly 4000 cal BP. Ages of the oldest corals above the unconformity are indicated. Below the unconformity, there are samples that are 200,000 yr or older (Taylor et al., forthcoming).

1996). For this work, we use the Cheng et al. (2000) revised ^{234}U and ^{230}Th half-lives for ^{230}Th -age and $\delta^{234}\text{U}$ determinations and adjusted marine value of $145.8 \pm 1.7\text{‰}$ for comparison to the coral $\delta^{234}\text{U}$ value.

As a second check for alteration, we dated corals older than 25,000 yr with high-precision ^{231}Pa -dating methods. The different isotopic systematics in ^{231}Pa and ^{230}Th dating allow ^{231}Pa ages to act as

an independent check on the ²³⁰Th age (Cheng et al. 1998). Samples that record concordant ²³⁰Th-²³¹Pa ages are significantly less likely to be altered. Ages are considered concordant when the ²³¹Pa ages are within ±2000 yr of the ²³⁰Th age and the 2-σ analytical errors are ≤2000 yr (Cutler et al. 2003).

RESULTS

Seventy-four corals were analyzed using paired ²³⁰Th-¹⁴C dating, 60 from Vanuatu and 14 from Papua New Guinea. Six of these samples were from surface exposures; the remainder were from drill cores. The ages of the corals range from 9 to 50 cal kyr BP; 11 of the samples record ages between 20 and 25 cal kyr BP, and 9 record ages older than 25 cal kyr BP. Eleven samples, including all nine with ages older than 25 cal kyr BP in addition to two others, were also dated with ²³¹Pa methods. The results, including isotopic composition, ¹⁴C, ²³⁰Th, and ²³¹Pa ages, and Δ¹⁴C values, are presented in Table 1. Table 1 also gives coral species, site location, and present elevation relative to sea level.

Screening for Sample Diagenesis

The δ²³⁴U_i results shown in Figure 4 reveal that the majority of analyses fall within 8‰ of the modern marine value (hatched box). We interpret the clustering of δ²³⁴U_i values as strong evidence that the modern marine δ²³⁴U value has been constant within bounds of 8‰ for the past several tens of thousands of years. Also, based on oceanic residence time arguments, there is reason to believe that marine δ²³⁴U should be constant within a percent or so over time scales of 10⁴ yr (Edwards et al. 2003; Edwards 1988; Richter and Turekian 1993; Hamelin et al. 1991; Henderson et al. 2002). For these reasons, we conclude that the 6 points that lie outside of the ±8‰ range have likely been altered, and we eliminate their ages from further consideration in this study.

The ²³⁰Th-²³¹Pa isotopic results shown in Figure 5 indicate that out of the 18 ²³¹Pa analyses (representing 11 samples), 4 analyses (2 samples) have ages that are discordant by more than 2000 yr. These samples are eliminated from further consideration in this study. The remaining data lie on or very close to concordia, evidence that those samples did not experience significant diagenetic shifts in the relevant isotope ratios. The concordia plot reveals the increased probability of diagenesis in older corals collected from surface exposures.

Plots of ¹⁴C age versus ²³⁰Th or calendar age between 6 and 14 kyr are presented in Figure 6. Samples from 3 Tasmaloum drill cores, 6A, 6B, and 7, are shown as inverted triangles; samples from the other cores are shown as solid circles. The 29 samples from the other cores agree within error with the IntCal98 spline, with only 1 sample slightly removed. A number of samples from cores 6A, 6B, and 7, however, lie outside this spline in a time interval when the spline is well constrained with high-resolution data (Kromer and Spurk 1998; Hughen et al. 1998; Bard et al. 1990, 1993, 1996, 1998; Edwards et al. 1993; Burr et al. 1998). This suggests that samples from the 6A, 6B, and 7 cores were more susceptible to diagenesis than samples from the other cores. Figure 4 shows that several of these same samples have unusually low δ²³⁴U_i values relative to the bulk of samples in the same time range, adding support to this conclusion.

To understand why Tasmaloum cores 6A, 6B, and 7 may have been more susceptible to alteration, the location of these cores was examined (Figures 2b and 3a). The cores lie more than a kilometer away from the other Tasmaloum site where cores 9A–L were collected. Moreover, they were drilled significantly further inland and from a significantly higher elevation (Figure 3a, Appendix) than any of the other 17 cores, with the exception of 9C. These observations suggest that corals at this site

Table 1 U, Th, Pa, and ¹⁴C analytical results.

Sample ^a	Sp ^b	E ^v (m)	²³⁸ U (ug/g)	²³² Th (pg/g)	[²³⁰ Th/ ²³⁸ U]	δ ²³⁴ U _m ^d (%)	²³⁰ Th age ^c (BP)	δ ²³⁴ U _f ^f (%)	δ ²³⁴ U _g ^g	Avg ²³⁰ Th age ^h (BP)	¹⁴ C age ^{e,corr} ^h (BP)	Anat ⁱ	Δ ¹⁴ C (‰)
<i>Tasmatoum samples</i>													
6A b, 15.5–17	?	13 (1)	2.984 (2)	323 (3)	0.0901 (3)	145.3 (1.1)	8927 (32)	149.0 (1.1)	P	8927 (32)	8150 (80)	4	68 (11)
6A a, 15.5–17 (A)	?	13 (1)	3.130 (2)	1079 (2)	0.0920 (2)	141.5 (1.2)	9158 (27)	145.2 (1.2)	P	9131 (19)	8150 (70)	5	94 (10)
6A 19–19.5 (A)	P	10 (1)	2.916 (16)	475 (53)	0.0914 (3)	141.5 (1.2)	9056 (67)	145.6 (1.2)	P	9160 (21)	8540 (80)	5	46 (11)
6A 19–19.5 (B)			2.897 (2)	21 (81)	0.0914 (7)	141.2 (1.2)	9101 (72)	144.9 (1.2)	P				
6A 19–19.5 (C)			2.908 (2)	38 (12)	0.0922 (2)	141.7 (1.3)	9178 (23)	145.4 (1.3)	P				
6B b<13	?	17 (1)	3.518 (2)	93 (22)	0.0784 (3)	144.2 (1.1)	7740 (31)	147.4 (1.1)	P	7740 (31)	6970 (50)	8	71 (8)
6B 14.5–16	?	14 (1)	2.815 (2)	32 (29)	0.0859 (5)	144.7 (1.1)	8505 (51)	148.2 (1.1)	P	8505 (51)	7580 (90)	2	89 (14)
6B 31.0–34.0 (A)	A	-3 (2)	3.891 (2)	82 (2130)	0.1008 (6)	131.3 (1.1)	10,174 (60)	135.1 (1.1)	F	10,973 (67)	10,250 (110)	3	53 (17)
6B 31.0–34.0 (B)			3.896 (3)	93 (680)	0.1002 (3)	129.5 (2.1)	10,121 (38)	133.3 (2.2)	F				
6B 31.0–34.0 (C)			3.983 (4)	103 (12)	0.1089 (6)	136.5 (1.4)	10,973 (67)	140.8 (1.4)	P				
6B 38.3–42.0 (A)	A	-11 (2)	3.704 (2)	114 (15)	0.1206 (4)	138.8 (1.2)	12,193 (43)	143.7 (1.2)	P	12,299 (28)	11,720 (100)	4	29 (13)
6B 38.3–42.0 (B)			3.620 (3)	105 (3)	0.1207 (5)	138.0 (1.3)	12,221 (54)	142.8 (1.3)	P				
6B 38.3–42.0 (C)			3.743 (1)	43 (12)	0.1238 (5)	138.9 (1.2)	12,539 (53)	143.9 (1.2)	P				
7 b>14, <<15	?	-1 (1)	2.564 (2)	101 (15)	0.1034 (3)	139.4 (1.1)	10,441 (31)	143.1 (1.2)	P	10,441 (31)	9670 (120)	3	61 (16)
7 a>14, <<15 (A)	?	-1 (1)	2.614 (2)	509 (2)	0.1040 (3)	138.9 (1.2)	10,441 (31)	143.1 (1.2)	P	10,419 (21)	9720 (100)	3	52 (13)
7 a>14, <<15 (B)			2.651 (1)	607 (17)	0.1035 (3)	137.0 (1.1)	10,399 (29)	141.1 (1.1)	P				
7 15–16	Fd	-2 (1)	2.654 (2)	18 (10)	0.1151 (5)	138.7 (1.2)	11,616 (52)	143.3 (1.2)	P	11,616 (52)	9830 (100)	4	199 (17)
7 19.8–20(a)	A	-7 (1)	3.495 (2)	225 (4)	0.1151 (5)	139.6 (1.2)	11,606 (52)	144.2 (1.2)	P	11,606 (52)	10,310 (70)	4	128 (12)
7 22–29(b) (A)	A	-12 (4)	3.676 (3)	20 (10)	0.1363 (7)	138.4 (1.2)	13,894 (73)	143.9 (1.2)	P	13,874 (39)	12,610 (120)	3	115 (17)
7 22–29(b) (B)			3.673 (3)	38 (280)	0.1361 (4)	138.8 (1.3)	13,866 (46)	144.3 (1.3)	P				
9A 14+ (A)	D	-10 (1)	2.597 (2)	74 (10)	0.1249 (3)	141.1 (1.3)	12,626 (32)	146.2 (1.3)	P	12,640 (19)	10,650 (80)	5	225 (13)
9A 14+ (B)			2.596 (2)	72 (244)	0.1248 (4)	140.9 (1.6)	12,622 (46)	146.0 (1.7)	P				
9A 14+ (C)			2.625 (1)	77 (9)	0.1248 (6)	139.6 (1.3)	12,635 (63)	144.7 (1.3)	P				
9A 14+ (D)			2.618 (3)	76 (7)	0.1243 (3)	139.6 (1.6)	12,587 (38)	144.6 (1.7)	P				
9A 14+ (E)			2.605 (2)	68 (7)	0.1266 (5)	141.1 (1.2)	12,810 (53)	146.3 (1.2)	P				
9B 12.5–13.12 (c)	P	-9 (1)	2.974 (3)	629 (14)	0.1216 (4)	142.8 (1.0)	12,247 (44)	147.8 (1.0)	P	12,247 (44)	10,480 (95)	4	193 (15)
9B 18.48–19.15 (a) (A)	A	-15 (1)	3.679 (2)	367 (2)	0.1429 (6)	138.6 (1.2)	14,604 (69)	144.4 (1.2)	P	14,565 (44)	12,430 (80)	5	239 (14)
9B 18.48–19.15 (b) (B)			3.821 (2)	909 (21)	0.1424 (5)	139.2 (1.2)	14,537 (57)	145.0 (1.2)	P				
9C 15.20–16.65	A	-2 (1)	3.434 (3)	882 (1)	0.1100 (3)	141.2 (1.3)	11,045 (31)	145.7 (1.3)	P	11,045 (31)	9830 (80)	3	119 (12)
9C 22.7–24.2	A	-9 (1)	3.005 (1)	130 (4)	0.1271 (6)	139.2 (1.2)	12,886 (63)	144.4 (1.2)	P	12,886 (63)	11,160 (120)	2	185 (20)
9C 26.7–27.15 (A)	A	-13 (1)	3.046 (1)	46 (15)	0.1379 (4)	139.4 (1.2)	14,045 (42)	145.0 (1.2)	P	14,057 (34)	12,270 (70)	6	189 (11)
9C 26.7–27.15 (B)			3.266 (2)	205 (7)	0.1381 (5)	139.1 (1.2)	14,078 (56)	144.7 (1.2)	P				
9D 12.28–13.75	P	-6 (1)	2.597 (1)	127 (4)	0.1137 (3)	140.1 (1.3)	11,449 (37)	144.7 (1.3)	P	11,449 (37)	10,010 (80)	4	149 (13)
9D 15.28–16.65	A	-9 (1)	3.123 (5)	142 (8)	0.1203 (5)	140.1 (1.2)	12,151 (54)	145.0 (1.2)	P	12,151 (54)	10,270 (70)	6	211 (13)
9E 22.55–22.85 (A)	?	-15 (1)	2.883 (1)	30 (20)	0.1452 (4)	138.0 (1.1)	14,867 (47)	143.9 (1.1)	P	14,870 (42)	12,410 (90)	4	289 (16)
9E 22.55–22.85 (B)			3.220 (3)	69 (21)	0.1453 (8)	137.7 (1.3)	14,878 (88)	143.6 (1.4)	P				
9E 23.45–24.25 (B)	A	-16 (1)	3.026 (2)	109 (6)	0.1400 (6)	141.0 (1.4)	14,259 (67)	146.8 (1.5)	P	14,259 (67)	12,520 (110)	3	181 (19)
9E 24.25–25.75	A	-18 (1)	3.327 (2)	38 (9)	0.1489 (5)	137.2 (1.2)	15,278 (55)	143.3 (1.3)	P	15,278 (55)	13,060 (90)	4	249 (16)
9E 25.75–27.25 (A)	A	-19 (1)	3.458 (3)	957 (2)	0.1935 (5)	133.4 (1.2)	20,362 (58)	141.3 (1.3)	P	20,385 (53)	17,280 (160)	2	370 (29)
9E 25.75–27.25 (B)			2.296 (4)	311 (2)	0.1948 (11)	133.9 (1.2)	20,502 (132)	141.9 (1.3)	P				
9E 30.25–31.75	A	-24 (1)	2.917 (3)	841 (1)	0.2289 (8)	131.1 (1.8)	24,577 (101)	140.5 (1.9)	P	24,577 (101)	19,810 (200)	3	660 (46)

Table 1 U, Th, Pa, and ¹⁴C analytical results. (Continued)

Sample ^a	Sp ^b	E _v ^c (m)	²³⁸ U (ug/g)	²³² Th (pg/g)	[²³⁰ Th/ ²³⁸ U]	$\delta^{234}\text{U}_m$ (‰)	²³⁰ Th age ^e (BP)	$\delta^{234}\text{U}_f$ (‰)	$\delta^{234}\text{U}_f^g$	Avg. ²³⁰ Th age ^h (BP)	¹⁴ C age _{corr} ^h (BP)	A _{nat} ⁱ	$\Delta^{14}\text{C}$ (‰)
<i>Tasmatoum samples</i>													
9F 103	P	-11 (1)	2.636 (3)	1773 (6)	0.1264 (4)	140.8 (1.1)	12,740 (48)	146.0 (1.2)	P	12,740 (48)	10,766 (200)	6	222 (31)
9F 125	A	-15 (1)	3.519 (4)	168 (5)	0.1381 (5)	138.0 (1.0)	14,042 (53)	143.6 (1.1)	P	14,042 (53)	12,416 (180)	1	165 (27)
9F 139	A	-17 (1)	3.382 (4)	350 (7)	0.1457 (9)	138.5 (1.2)	14,866 (102)	144.5 (1.2)	P	14,866 (102)	12,681 (190)	1	246 (33)
9F 178	Fd	-24 (1)	2.743 (2)	3215 (8)	0.1957 (6)	134.1 (1.1)	20,559 (75)	142.1 (1.1)	P	20,559 (75)	17,936 (320)	1	289 (53)
9H 92	P	-13 (1)	3.353 (3)	3551 (12)	0.1208 (7)	139.9 (1.1)	12,157 (79)	144.8 (1.2)	P	12,157 (79)	10,296 (180)	2	208 (29)
9H 113 (a)	A	-18 (1)	3.287 (3)	1996 (9)	0.1392 (5)	137.5 (1.1)	14,169 (55)	143.1 (1.2)	P	14,221 (39)	12,276 (140)	1	212 (22)
(b)			3.317 (5)	2409 (15)	0.1404 (6)	137.9 (1.2)	14,298 (72)	143.6 (1.2)	P				
(c)			3.330 (5)	1332 (16)	0.1400 (8)	139.1 (1.3)	14,233 (86)	144.8 (1.3)	P				
9H 283 (A)	Fd	-29 (1)	3.658 (5)	4386 (38)	0.2025 (7)	131.6 (1.2)	21,406 (81)	139.8 (1.2)	P	21,568 (58)	18,496 (300)	1	359 (52)
(B)			3.907 (5)	1714 (7)	0.2052 (7)	130.6 (1.2)	21,739 (83)	138.9 (1.3)	P	13,959 (41)	12,050 (160)	1	207 (25)
9J 64 (A)	As	-16 (1)	3.095 (4)	1291 (15)	0.1371 (7)	138.7 (1.3)	13,928 (73)	144.3 (1.3)	P				
(B)			3.100 (3)	848 (11)	0.1376 (4)	139.4 (1.2)	13,973 (50)	145.0 (1.3)	P				
9J 81	A	-18 (1)	3.693 (4)	1184 (7)	0.1410 (6)	138.2 (1.1)	14,358 (66)	143.9 (1.1)	P	14,358 (66)	12,244 (210)	1	237 (34)
9J 87	?	-18 (1)	1.611 (2)	36 (3)	0.1379 (5)	135.3 (1.3)	14,059 (57)	140.8 (1.3)	P	14,059 (57)	12,426 (127)	2	166 (20)
9J 155	P	-27 (1)	3.532 (3)	1280 (7)	0.1874 (6)	133.2 (1.1)	19,623 (68)	140.8 (1.2)	P	19,623 (68)	17,166 (180)	2	267 (30)
9L 89	P	-15 (1)	2.705 (2)	253 (20)	0.1314 (15)	140.2 (1.1)	13,287 (166)	145.6 (1.2)	P	13,287 (166)	11,506 (140)	1	191 (32)
<i>Urelapa samples</i>													
10 42	P	-5 (1)	3.111 (4)	1073 (27)	0.0681 (4)	140.1 (1.1)	6675 (40)	142.8 (1.1)	P	6675 (40)	6017 (130)	1	60 (18)
10 48	P	-6 (1)	3.011 (4)	675 (19)	0.0697 (3)	140.3 (1.1)	6833 (35)	143.0 (1.1)	P	6833 (35)	6012 (95)	2	81 (14)
10 108	P	-16 (1)	3.026 (4)	50 (18)	0.0990 (3)	138.4 (1.1)	9873 (34)	142.4 (1.2)	P	9873 (34)	8803 (160)	16	103 (22)
10 128	P	-19 (1)	2.190 (3)	22 (23)	0.1047 (4)	139.8 (1.4)	10,457 (42)	144.0 (1.4)	P	10,457 (42)	9167 (100)	3	132 (15)
10 148	G	-24 (1)	2.384 (3)	10 (23)	0.1123 (5)	142.8 (1.0)	11,221 (52)	147.4 (1.1)	P	11,221 (52)	9732 (100)	2	157 (16)
10 152	L	-25 (1)	2.332 (2)	5832 (40)	0.1137 (5)	141.2 (1.1)	11,387 (50)	145.8 (1.2)	P	11,387 (50)	9777 (120)	1	174 (19)
10 160	P	-27 (1)	2.451 (3)	403 (28)	0.1167 (4)	142.0 (1.1)	11,698 (44)	146.8 (1.1)	P	11,698 (44)	10,092 (90)	4	172 (15)
10 194	A	-43 (1)	3.662 (5)	49 (20)	0.1554 (6)	137.9 (1.2)	15,945 (70)	144.3 (1.2)	P	15,945 (70)	13,332 (170)	1	309 (30)
10 209	Fd	-48 (1)	2.663 (3)	4224 (19)	0.2048 (8)	134.3 (1.2)	21,606 (101)	142.7 (1.3)	P	21,606 (101)	18,372 (300)	1	386 (54)
10 214	P	-49 (1)	2.725 (2)	53 (4)	0.2078 (6)	133.9 (1.1)	21,970 (76)	142.5 (1.2)	P	21,970 (76)	18,112 (180)	22	496 (36)
10 217	Fd	-50 (1)	2.735 (3)	6914 (57)	0.2104 (9)	134.7 (1.1)	22,260 (114)	143.4 (1.1)	P	22,260 (114)	18,782 (240)	1	425 (47)
10 221	P	-51 (1)	3.549 (5)	4405 (49)	0.2137 (6)	131.7 (1.4)	22,709 (76)	140.4 (1.5)	P	22,709 (76)	19,542 (400)	2	369 (69)
11 78	P	-25 (1)	2.670 (3)	2728 (21)	0.1125 (4)	146.6 (1.2)	11,208 (48)	151.3 (1.2)	P	11,208 (48)	9567 (130)	1	179 (20)
11 104	P	-35 (1)	2.654 (3)	1470 (18)	0.1250 (4)	142.4 (1.0)	12,610 (49)	147.6 (1.0)	P	12,610 (49)	10,806 (32)	18	197 (9)
12 106	P	-22 (1)	2.677 (3)	1303 (9)	0.1127 (3)	140.2 (1.1)	11,288 (37)	144.8 (1.1)	P	11,288 (37)	9727 (140)	1	167 (21)
13 48	P	-13 (1)	2.412 (2)	120 (2)	0.0633 (3)	145.4 (1.1)	6150 (28)	148.0 (1.2)	P	6150 (28)	5382 (100)	1	77 (14)
13 60	P	-21 (1)	2.570 (2)	108 (4)	0.0882 (3)	142.3 (1.4)	8719 (33)	145.8 (1.4)	P	8719 (33)	7897 (110)	1	74 (15)
13 74/75 (a)	P	-24 (1)	2.524 (2)	1368 (5)	0.0974 (3)	141.6 (1.0)	9679 (29)	145.5 (1.0)	P	9679 (29)	8522 (130)	1	116 (18)
(b)			2.579 (3)	1569 (8)	0.0975 (3)	142.2 (1.3)	9681 (32)	146.2 (1.3)	P				
13 85	A	-30 (1)	3.455 (5)	449 (25)	0.1157 (10)	138.7 (1.2)	11,632 (107)	143.4 (1.2)	P	11,632 (107)	9982 (160)	1	179 (28)
13 88	P	-34 (1)	2.768 (4)	181 (23)	0.1253 (6)	140.9 (1.1)	12,630 (68)	146.0 (1.2)	P	12,630 (68)	10,977 (240)	1	175 (36)
13 130	Fd	-52 (1)	2.831 (3)	23 (21)	0.2083 (8)	129.6 (1.1)	22,127 (98)	137.9 (1.2)	P	22,127 (98)	18,802 (300)	1	399 (55)
14 54	P	-24 (1)	2.409 (3)	1730 (12)	0.1031 (4)	139.2 (1.7)	10,296 (44)	143.3 (1.7)	P	10,296 (44)	9143 (136)	1	113 (20)
14 127	D	-56 (1)	2.638 (3)	3360 (17)	0.2138 (12)	133.1 (1.3)	22,690 (139)	142.0 (1.4)	P	22,690 (139)	19,602 (280)	2	356 (53)

Table 1 U, Th, Pa, and ¹⁴C analytical results. (Continued)

Sample ^a	Sp ^b	E _v ^c (m)	²³⁸ U (ug/g)	²³² Th (pg/g)	[²³⁰ Th/ ²³⁸ U] (%)	^{δ²³⁴U_m} ^d (%)	²³⁰ Th age ^e (BP)	^{δ²³⁴U_f} (%)	^{δ²³⁴U_g} (%)	Avg ²³⁰ Th age ^h (BP)	¹⁴ C age ^{cor^h} (BP)	Δ ¹⁴ C ^j (‰)	[²³¹ Pa/ ²³⁵ U] (BP)	²³¹ Pa age ^k (BP)
<i>Papua New Guinea samples</i>														
GT 38.0	A	-33 (1)	3.355 (3)	286 (9)	0.1233 (6)	141.3 (1.2)	12,449 (64)	146.4 (1.2)	P	12,449 (64)	10,420 (220)	232 (35)	0.238 (5)	12,800 (300) P
GT 40.95	A	-35 (1)	2.390 (3)	9292 (143)	0.1251 (7)	141.8 (1.2)	12,542 (130)	146.9 (1.3)	P	12,542 (130)	10,530 (125)	229 (27)	0.238 (5)	12,800 (300) P
KNM 46.7	?	-41 (1)	2.840 (3)	249 (5)	0.1431 (5)	139.8 (1.2)	14,611 (52)	145.7 (1.2)	P	14,611 (52)	12,390 (240)	252 (38)	0.401 (3)	24,200 (200) P
KNM 50.0 (B)	?	-45 (1)	3.275 (3)	1058 (11)	0.2212 (8)	130.8 (1.2)	23,662 (96)	139.8 (1.2)	P	23,644 (66)	19,420 (280)	557 (56)	0.407 (5)	24,700 (400) P
KNM 58.7 (A)	P	-53 (1)	3.278 (3)	1000 (7)	0.2212 (7)	132.2 (1.3)	23,628 (90)	141.4 (1.3)	P	25,292 (66)	20,130 (110)	739 (28)	0.426 (9)	26,200 (800) P
KNM (B)	?	2.219 (3)	2.424 (3)	112 (7)	0.2346 (7)	136.2 (1.1)	25,134 (90)	146.3 (1.2)	P	36,790 (182)	32,700 (640)	462 (121)	0.536 (15)	36,300 (1600) P
KNM T-2 * (a)	?	2.527 (3)	2.527 (3)	1936 (16)	0.3240 (14)	125.7 (1.2)	36,796 (201)	139.5 (1.4)	P	46,448.4 (181)	34,610 (620)	2706 (298)	0.612 (5)	45,110 (947) P
KNM (b)	?	2.989 (3)	2.989 (3)	2301 (28)	0.3242 (31)	127.2 (1.1)	36,763 (423)	141.1 (1.3)	P	48,469.4 (143)	34,000 (1280)	4106 (822)	0.552 (9)	49,000 (1000) P
KWA 41.24	?	-36 (1)	2.312 (3)	80 (16)	0.1278 (9)	141.4 (7.2)	12,938 (126)	146.7 (7.4)	P	50,630 (221)	46,000 (2600)	489 (492)	0.645 (7)	49,000 (1000) P
KWA 60.2	?	-55 (1)	3.988 (5)	739 (16)	0.2508 (6)	131.9 (1.6)	27,208 (91)	142.4 (1.8)	P	48,758 (362)	36,890 (1920)	2690 (905)	0.625 (10)	50,800 (1200) P
KWA 64.3 (B)	?	-58 (1)	3.146 (4)	3907 (94)	0.2619 (13)	128.7 (1.2)	28,645 (169)	139.5 (1.3)	F	48,565 (318)	43,200 (2600)	643 (545)	0.485 (9)	31,326 (860) F
KWA 1-1* (A)	P	9 (2)	3.479 (6)	4197 (51)	0.2629 (14)	135.8 (1.3)	28,564 (177)	147.2 (1.4)	P	46,448.4 (181)	34,610 (620)	2706 (298)	0.615 (8)	45,110 (947) P
KWA (B)	P	2.902 (3)	2.902 (3)	61 (8)	0.3921 (30)	120.1 (1.3)	46,643 (445)	137.0 (1.4)	F	48,758 (362)	36,890 (1920)	2690 (905)	0.625 (10)	50,800 (1200) P
KWA K-1* (A)	P	30 (2)	2.943 (4)	160 (24)	0.3902 (13)	119.4 (1.2)	46,410 (197)	136.2 (1.3)	F	48,469.4 (143)	34,000 (1280)	4106 (822)	0.605 (12)	43,926 (1461) F
KWA (B)	P	9 (2)	3.355 (4)	51 (5)	0.4128 (13)	119.0 (1.2)	49,807 (203)	137.0 (1.3)	F	50,630 (221)	46,000 (2600)	489 (492)	0.645 (7)	49,000 (1000) P
KWA N-1* (A)	P	9 (2)	3.623 (4)	173 (5)	0.3945 (13)	116.9 (1.1)	47,178 (200)	133.5 (1.2)	F	48,758 (362)	36,890 (1920)	2690 (905)	0.625 (10)	50,800 (1200) P
KAN D-4* (B)	P	75 (2)	2.744 (4)	62 (9)	0.4202 (17)	121.1 (1.2)	50,798 (263)	139.8 (1.4)	P	48,565 (318)	43,200 (2600)	643 (545)	0.485 (9)	31,326 (860) F
KAN C-2* (B)	F	45 (2)	2.321 (3)	497 (19)	0.4054 (21)	121.1 (1.1)	48,565 (318)	138.9 (1.2)	P	48,565 (318)	43,200 (2600)	643 (545)	0.485 (9)	31,326 (860) F

^a Numbers in left column identify Vanuatu drill cores; letters identify New Guinea collection sites: KNM = Kanoni, KWA = Kwambu, KAN = Kanzaru, GP = Gagidu Point. Replicates denoted with (A), (B),... are fragments of the same sample and (a), (b),... are aliquots of the same sample split. * identifies samples collected from surface exposures.

^b Genus: A = *Acropora* sp., As = *Astreopora*, D = *Diploastrea*, Fd = *Favosites*, G = *Goniopora* sp., L = *Leptastrea*, and P = *Porites* sp.

^c Present elevation relative to sea level.

^d ^{δ²³⁴U_m} is the measured ^{δ²³⁴U} value.

^e ²³⁰Th ages calculated from the equation $(^{230}\text{Th}/^{238}\text{U}) - 1 = -\exp(-\lambda_{230}T) + (\delta^{234}\text{U}_m/1000)[\lambda_{230}/(\lambda_{230} - \lambda_{234})][1 - \exp(\lambda_{234} - \lambda_{230})T]$, where T is the age, $\lambda_{230} = 9.1577 \times 10^{-6} \text{ yr}^{-1}$, and $\lambda_{234} = 2.8263 \times 10^{-6} \text{ yr}^{-1}$ (Cheng et al. 2000).

^f $\delta^{234}\text{U}_f = \delta^{234}\text{U}_m \exp(\lambda_{230}T)$.

^g $\delta^{234}\text{U}_c = \delta^{234}\text{U}_f$ screening criteria and ²³¹Pa_c = ²³¹Pa screening criteria defined in text; P indicates the sample passed and F indicates the sample failed the screening criteria.

^h Ages from replicate samples are weight averaged; ages in **bold** are from samples that passed all screening criteria (see text). ¹⁴C ages are reservoir corrected: 400 yr for New Guinea and Urelapa samples, 500 yr for Tasmaloum samples.

ⁱ Number of ¹⁴C measurements on separate subsamples.

^j $\Delta^{14}\text{C} = [F_{\text{RC}} \exp(\lambda t - 1)]/1000$, where t is the ²³⁰Th age, $\lambda = 1/8267 \text{ yr}^{-1}$, and F_{RC} is the reservoir-corrected fraction of modern carbon (Burr et al. 1998).

^k ²³¹Pa ages are calculated from the equation $T = -\ln[1 - (\delta^{231}\text{Pa}/^{235}\text{U})/\lambda_{231}]$, where $\lambda_{231} = 2.11583 \times 10^{-5} \text{ yr}^{-1}$ (Robert et al. 1969).

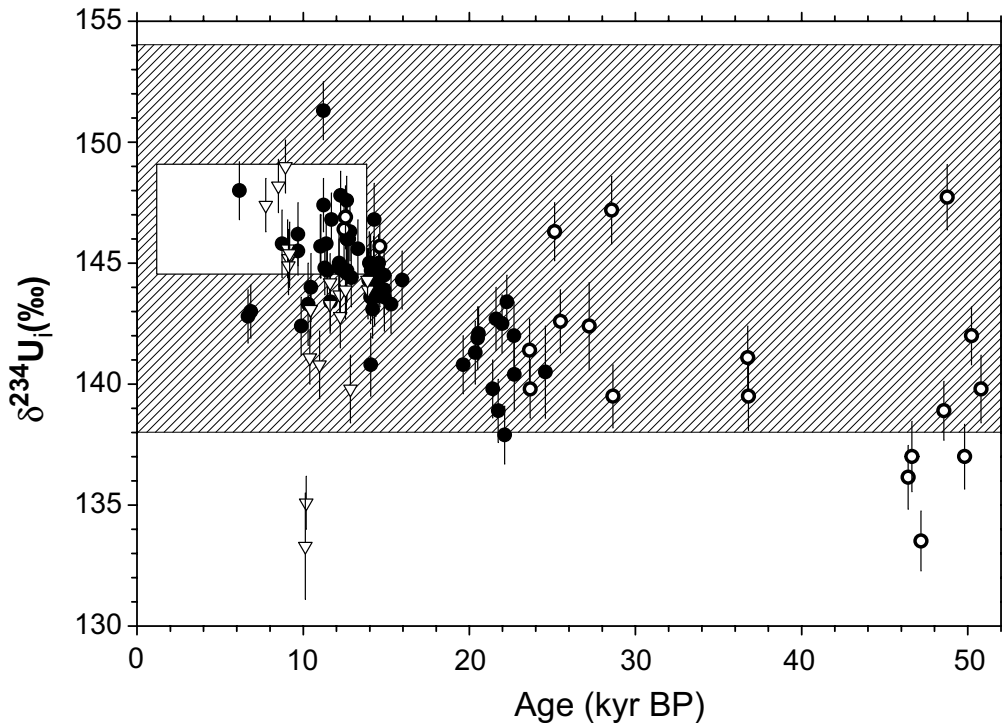


Figure 4 $\delta^{234}\text{U}_i$ versus age diagram. Inverted triangles are data from cores 6A, 6B, and 7; solid circles are data from other Vanuatu cores; and open circles are data from Papua New Guinea. Plots include replicate analyses. Error bars are 2σ and, if not visible, are smaller than the symbol. The envelope with hatch marks indicates boundaries of $\delta^{234}\text{U}_i$ screening criteria: $146 \pm 8\text{‰}$. The open envelope delineates earlier coral $\delta^{234}\text{U}_i$ results from Papua New Guinea (Edwards et al. 1993) and provides the marine reference value for that period (see text).

may have been more susceptible to alteration. This may have resulted because the environment surrounding this particular locality was anomalously conducive to diagenesis, or more likely, because the greater distance both horizontally and vertically from the sea allowed greater interaction with meteoric water over longer periods of time. Based on these arguments, we eliminated samples from cores 6A, 6B, and 7 from further consideration in this study. Our continued discussion focuses on the 17 other drill cores that show little evidence of diagenetic alteration.

Calibration Results

The screened calibration data, derived from corals which record marine $\delta^{234}\text{U}$ values that give concordant ^{231}Pa and ^{230}Th ages (for samples analyzed with ^{231}Pa) and are acquired from drill cores with little evidence of alteration, are shown in Figures 7 and 8. Replicate analyses were combined using a weighted average.

The results show that the coral data that overlap in the range of the tree-ring calibration (represented by the IntCal98 envelope) are in close agreement (Figure 8a). Thirteen calibration points extend beyond the tree-ring calibration to 14 cal kyr BP. The close agreement between these points and the IntCal98 spline confirms the data upon which this portion of the spline is based (Hughen et al. 1998; Bard et al. 1990, 1993, 1996, 1998; Edwards et al. 1993; Burr et al. 1998).

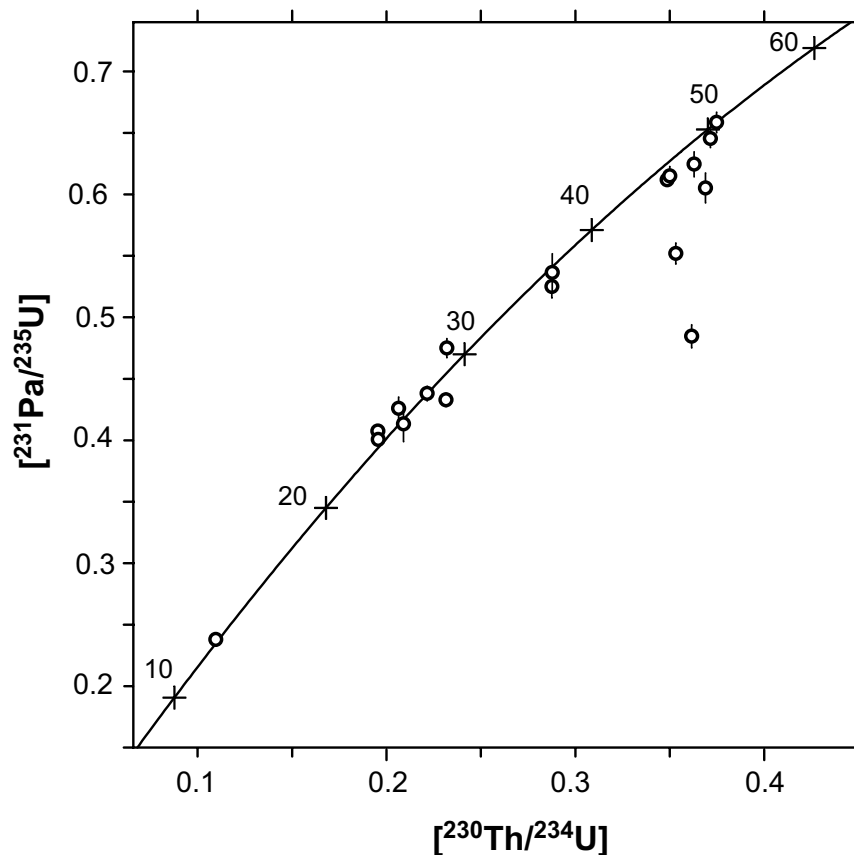


Figure 5 ^{231}Pa - ^{230}Th concordia diagram. $[^{231}\text{Pa}/^{235}\text{U}] - [^{230}\text{Th}/^{234}\text{U}]$ concordia diagram of samples analyzed for ^{231}Pa . All samples are from Papua New Guinea; error bars are 2σ and, if not visible, are smaller than the symbol. The curved line, "concordia," shows equal ^{231}Pa - ^{230}Th age values. Crosses on concordia indicate age in thousands of years (kyr).

In addition, 23 calibration points fall between 14 and 24 cal kyr BP, an interval in which, prior to this work, there were few data points. The new points provide detailed structure for the intervals between 14 and 16 cal kyr BP and between 19 and 24 cal kyr BP. Two of these samples, with ages of 12.5 and 23.6 cal kyr BP, were also analyzed for ^{231}Pa and produced concordant ^{230}Th - ^{231}Pa ages.

Finally, 6 samples range in age from 24 cal kyr BP to the limit of ^{14}C dating, 50 cal kyr BP. The 5 samples older than 25 cal kyr BP are ^{230}Th - ^{231}Pa age concordant and were ^{14}C dated multiple times (Table 1). The rigorous analysis of these samples lends significant credence to the extension of the calibration presented here.

The results, in general, show that the offset between calibrated and ^{14}C ages generally increases with age until about 28 cal kyr BP. At 14 cal kyr BP, the ^{14}C age is about 1600 yr too young, and at 28 cal kyr BP, the ^{14}C age is about 6800 yr too young. The 2 points prior to 28 cal kyr BP indicate less of a gap between the calibrated and ^{14}C age. At 37 cal kyr BP, the ^{14}C age is about 4000 yr too young, and at 50 cal kyr BP, the ^{14}C age is about 4600 yr too young. This older trend is supported by the solitary point of Bard et al. (1990a) that shows an age gap of 4000 yr at 30 cal kyr BP.

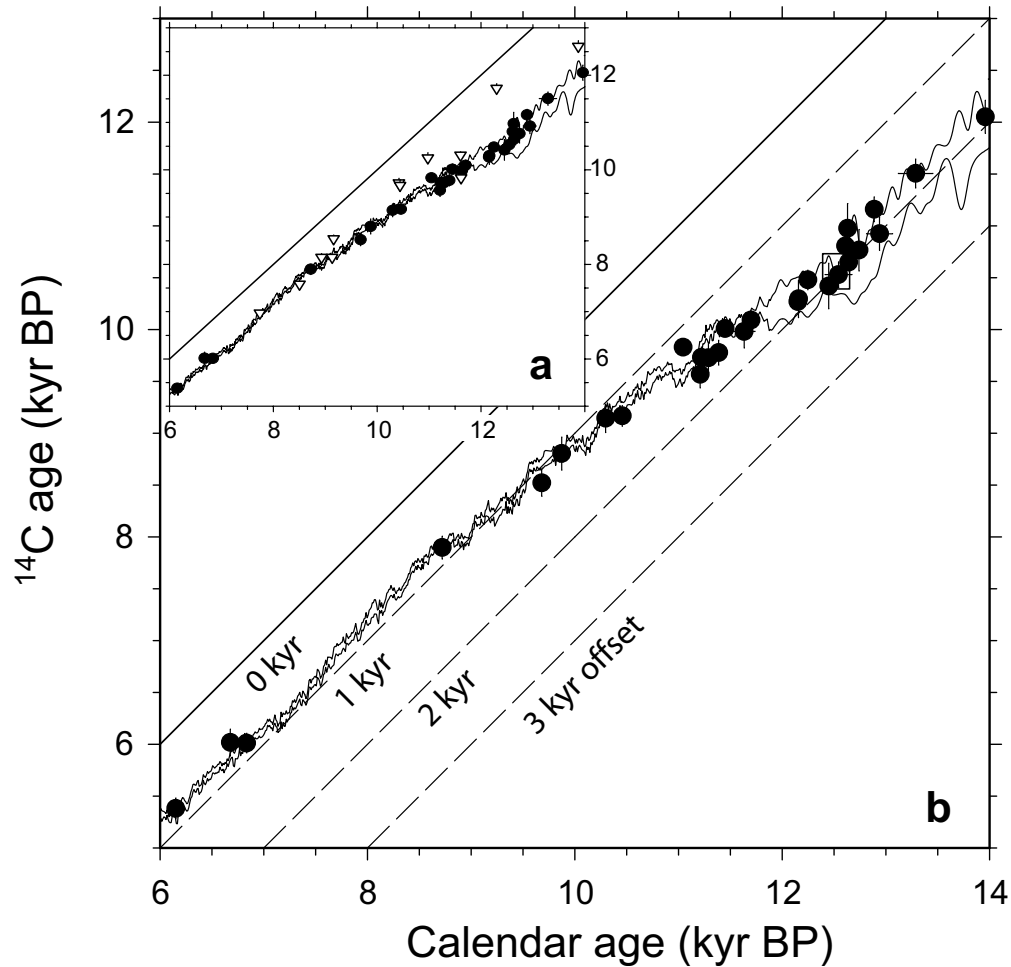


Figure 6 Screening for drill core diagenesis. Calibration results between 6 and 14 cal kyr BP. Curved lines are the IntCal98 calibration envelope; inverted triangles are data from cores 6A, 6B, and 7; and solid circles are data from all other cores. In this age range, only 1 sample was analyzed for ²³¹Pa. This sample gives concordant ²³⁰Th-²³¹Pa ages and is marked with a box at 12.5 cal kyr BP. Error bars are 2 σ and, if not visible, are smaller than the symbol. Diagonal line is the one-to-one reference line of equal age; parallel dashed lines show 1000-yr offset lines. All data between 6–14 cal kyr BP are shown in (a) and data set after removal of data from drill cores showing evidence of diagenesis are shown in (b) (see text).

Significantly, the new data reveals 2 major ¹⁴C age plateaus that prevent precise ¹⁴C dating during these times. The first age plateau lasts for 1000 yr, between 14.9 and 13.9 cal kyr BP, and gives a nearly constant ¹⁴C age of 12.4 ± 0.2 kyr BP (Figure 9) associated with a $\Delta^{14}\text{C}$ drop (Figure 10). The second, longer age plateau extends for 3000 yr, between 25 and 22 cal kyr BP, and gives a uniform ¹⁴C age of 19.8 ± 0.3 kyr BP (Figure 11) associated with a $\Delta^{14}\text{C}$ drop (Figure 12).

For the most part, the Lake Suigetsu varved sediment record of Kitagawa and van der Plicht (2000; Figure 8, small triangles) compares well with the coral record. However, it disagrees between 25 and 28 cal kyr BP, the timing of the larger ¹⁴C age plateau. This discrepancy between the 2 records is plausibly due to missing varves or the assumption of constant sedimentation rate for portions of the record. The younger portion of the Bahamas speleothem record of Beck et al. (2001; Figure 8, grey envelope) also agrees well with the coral record. However, because the speleothem record has a gap

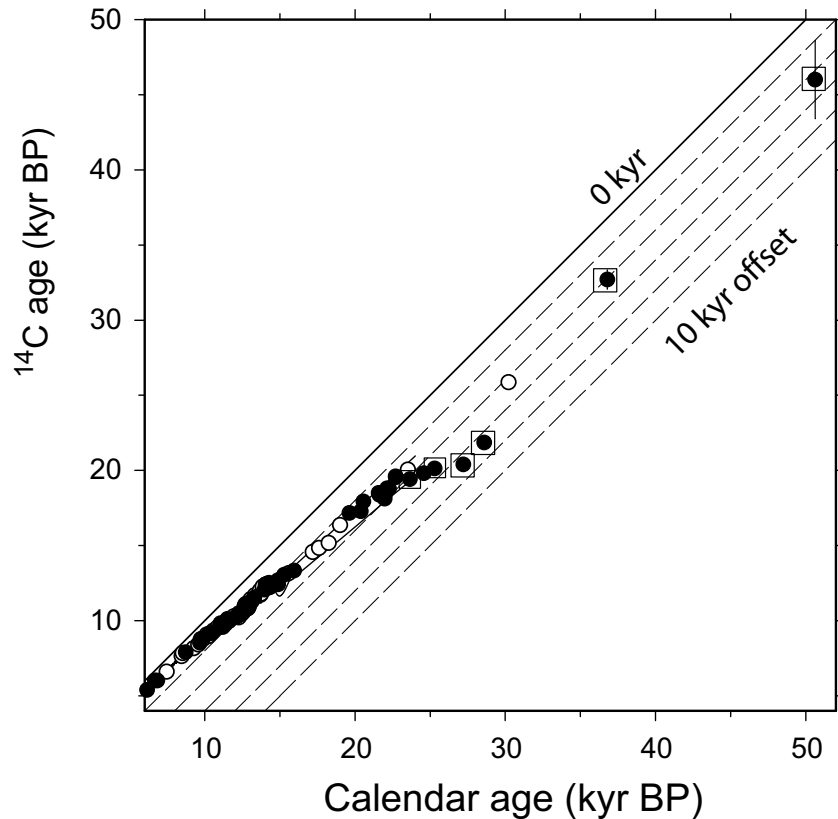


Figure 7 Coral calibration results between 6 and 50 cal kyr BP. Solid circles are screened coral data from this study. ^{230}Th - ^{231}Pa age-concordant samples are marked with a box. Open circles represent existing coral calibration data (Bard et al. 1990, 1993, 1998 in this time range) for corals that record marine $\delta^{234}\text{U}$ values according to $\delta^{234}\text{U}_i$ criteria (see text). Parallel dashed lines indicate 2000-yr offset lines from solid line of equal age. Error bars are 2σ and, if not visible, are smaller than the symbol.

between 26 and 28 cal kyr BP, a comparison cannot be made during the timing of the larger ^{14}C plateau. There is a discrepancy between the 2 records of more than 1500 yr at the 37-cal kyr BP coral point. This discrepancy could be due to the assumption of a constant dead carbon fraction in the speleothem record.

DISCUSSION

^{14}C Age Plateau: 14–15 cal kyr BP

Figure 9 shows the tree-ring and coral calibration data between 10 and 16 cal kyr BP and the corresponding atmospheric $\Delta^{14}\text{C}$ record. The new findings are in close agreement with the earlier data and support the previously identified ^{14}C plateau between 12.5 and 11.5 cal kyr BP (Edwards et al. 1993; Goslar et al. 1995; Hughen et al. 1998). In addition, the new results reveal a second plateau between 15 and 14 cal kyr BP. This plateau, resulting from a 130% drop in atmospheric $\Delta^{14}\text{C}$, compresses the ^{14}C time scale such that all materials between 14.9 and 13.9 kyr old give nearly the same ^{14}C age: 12.4 ± 0.2 kyr BP. This has repercussions for ^{14}C dating: the ^{14}C time scale does not allow for precise ^{14}C age determinations over this interval.

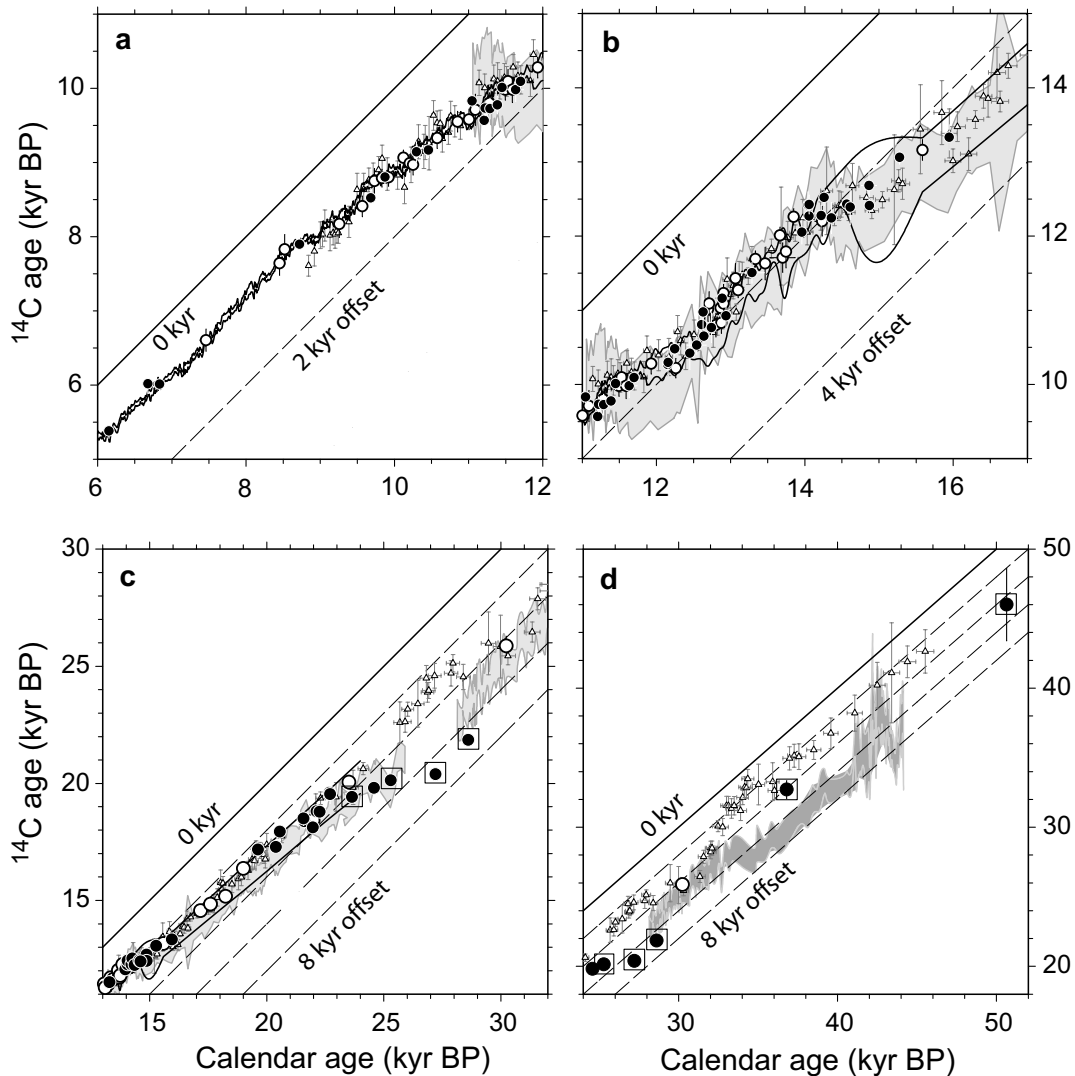


Figure 8 Details of coral calibration results. Calibration results between 6 and 12 cal kyr BP (a), 11 and 17 cal kyr BP (b), 13 and 32 cal kyr BP (c), and 24 and 52 cal kyr BP (d). Symbols are the same as in Figure 7. In addition, curved lines are the IntCal98 calibration envelope, small triangles represent the Lake Suigetsu varved sediment record of Kitagawa and van der Plicht (2000), and the gray shaded envelope represents the Bahamas speleothem record of Beck et al. (2001). Parallel dashed lines indicate 2000-yr offset lines from the solid line of equal age. Error bars are 2σ .

An enlargement of the 15–14-cal kyr BP plateau is shown in Figure 9c. In addition to the new results, the plot includes the IntCal98 envelope and the previous coral and marine varve data that were used to establish the IntCal98 spline in this interval. While the new data are in good agreement with the original data, the IntCal98 envelope does not “see” the plateau and crosses diagonally through it. This points to the clear need for higher-resolution records.

Several studies propose that the drop in atmospheric $\Delta^{14}\text{C}$ associated with a later ¹⁴C plateau, between 12.5 and 11.5 cal kyr BP, was caused by changes in the carbon cycle likely associated with the Younger Dryas climate event (Edwards et al. 1993; Goslar et al. 1995; Hughen et al. 1998;

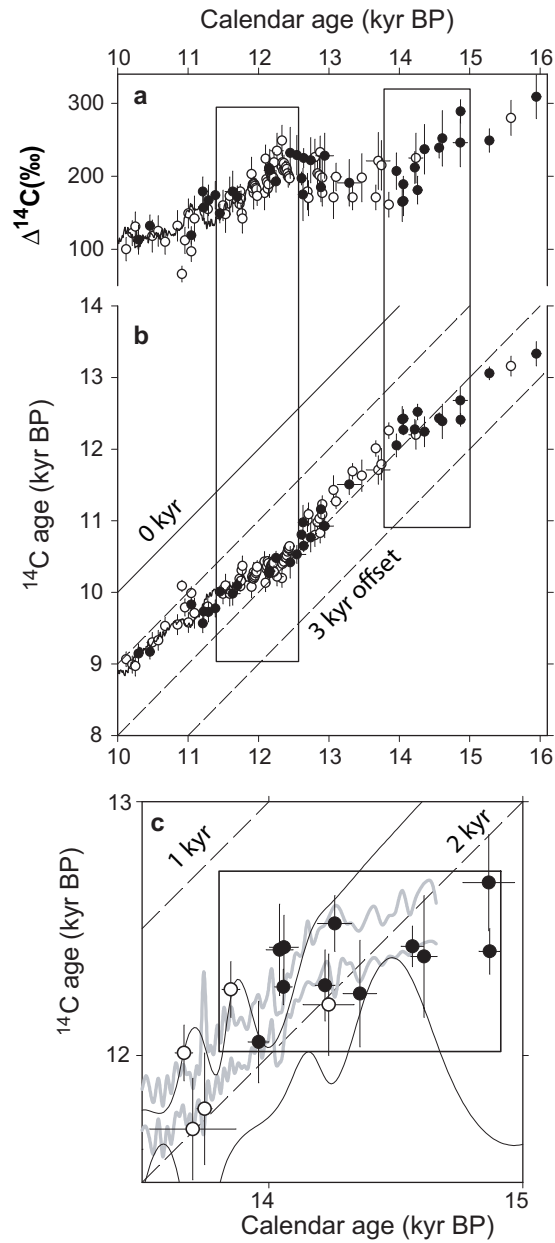


Figure 9 ^{14}C age plateau between 14–15 cal kyr BP. Solid circles are data from this study, open circles are from previous coral records (Bard et al. 1990, 1993, 1996, 1998; Edwards et al. 1993; Burr et al. 1998; data were screened with the $\delta^{234}\text{U}_i$ criteria), and the jagged line is the tree-ring calibration (Kromer and Spurk 1998). Parallel dashed lines indicate 1000-yr offset lines from solid diagonal line of equal age. Rapid drops in the atmospheric $\Delta^{14}\text{C}$ record between 10 and 16 cal kyr BP (a), and corresponding ^{14}C age plateaus in the calibration (b), are marked with boxes. The data support the previously identified plateau between 11.5 and 12.5 cal kyr BP and reveal a second plateau between 14 and 15 cal kyr BP. An enlargement of the 14–15-cal kyr BP plateau (d) includes the Cariaco Basin varved sediment record (grey 2- σ envelope, Hughen et al. 2000) and the IntCal98 calibration (black envelope). All error bars are 2 σ .

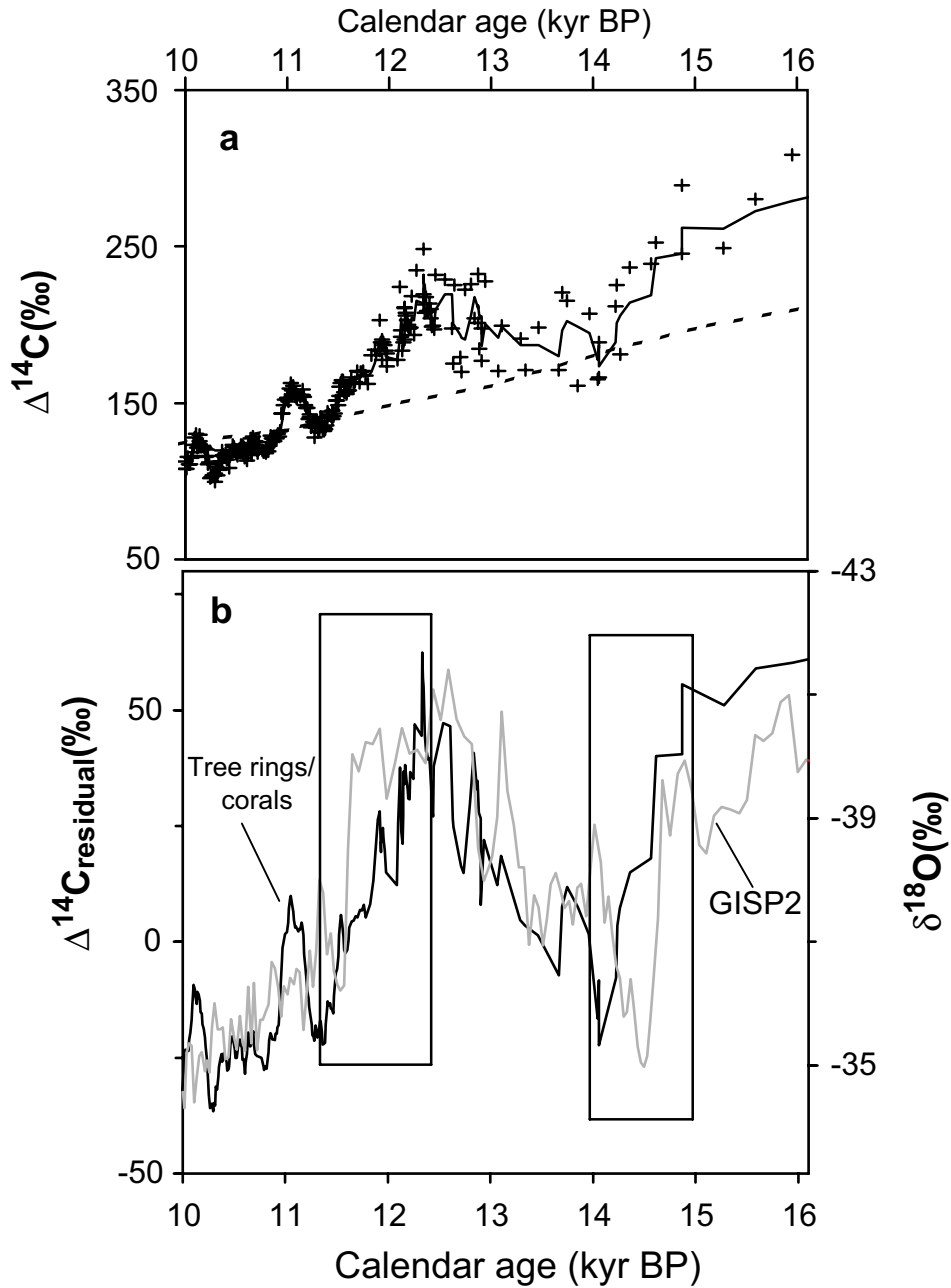


Figure 10 Atmospheric $\Delta^{14}\text{C}$ and the GISP2 $\delta^{18}\text{O}$ record, 10–16 cal kyr BP. (a) Crosses are a combined atmospheric $\Delta^{14}\text{C}$ data set based on tree rings after 11.9 cal kyr BP and corals (this study and previous records, see Figure 9) prior to 11.9 cal kyr BP. Jagged solid line is 3-point running average of this data set; dashed line represents $\Delta^{14}\text{C}$ values expected from changes in geomagnetic field intensity (Guyodo and Valet 1996). (b) Solid line is the 3-point running average from (a) with the geomagnetic trend subtracted out (see text). Gray line is the GISP2 oxygen isotope record (Grootes et al. 1997). Boxes mark the times of the ^{14}C age plateaus shown in Figure 9.

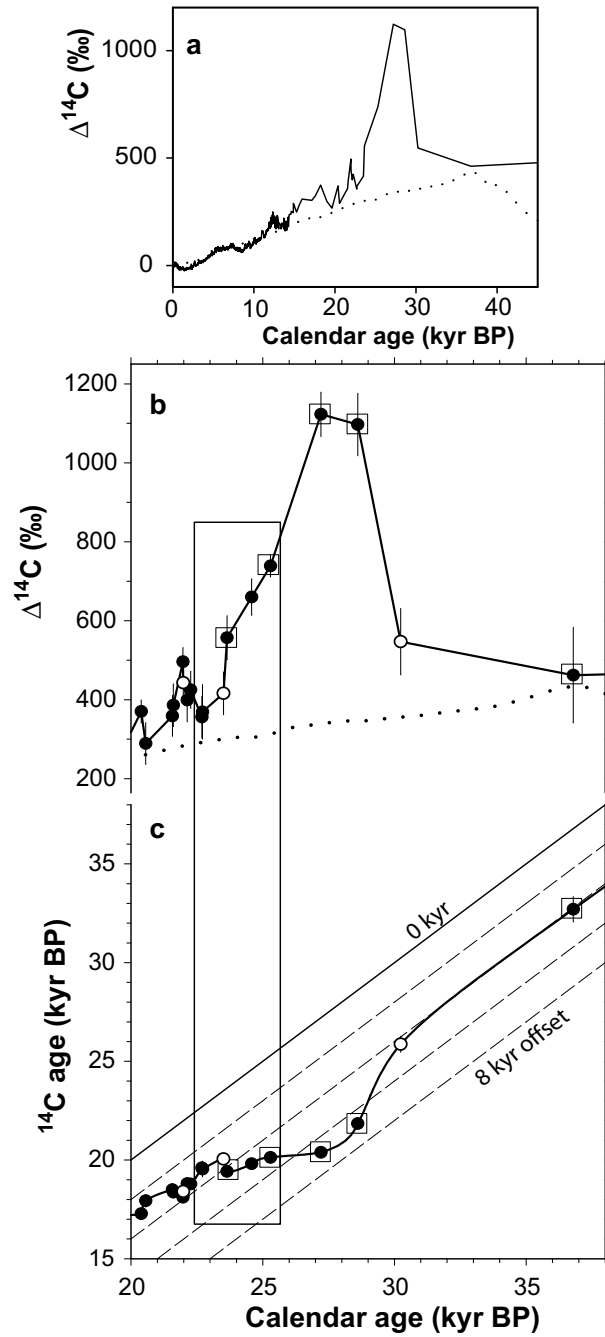


Figure 11 $\Delta^{14}\text{C}$ excursion at 28 cal kyr BP. Line connects tree-ring data, coral data from this study (solid circles), and coral data from previous records (open circles; Bard et al. 1990, 1993, 1996, 1998). All errors are 2σ . Boxes around symbols indicate samples with concordant ^{230}Th - ^{231}Pa ages. Dotted line represents $\Delta^{14}\text{C}$ values expected from changes in geomagnetic field intensity. The rectangle identifies timing of plateau. (a) Atmospheric $\Delta^{14}\text{C}$ record between 0 and 45 cal kyr BP showing long-term geomagnetic contribution to $\Delta^{14}\text{C}$ values. (b) Excursion and subsequent drop in atmospheric $\Delta^{14}\text{C}$ causing ^{14}C age plateau in calibration (c).

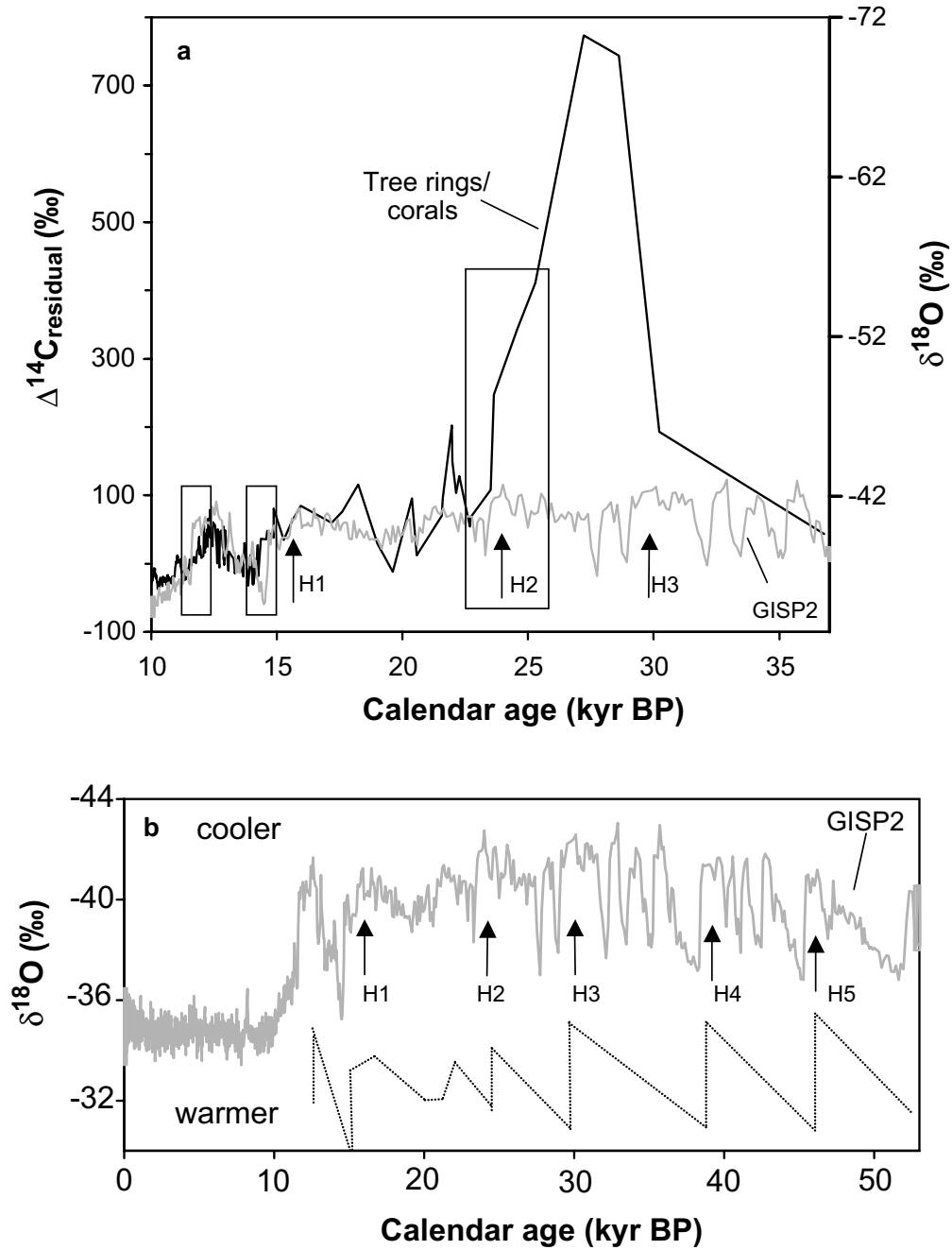


Figure 12 Atmospheric $\Delta^{14}\text{C}$ and the GISP2 $\delta^{18}\text{O}$ record, 10–37 cal kyr BP. (a) Dark line is the tree-ring and coral data, as in Figure 11; gray line is the GISP2 oxygen isotope record. H1,2,... indicate the timing of Heinrich events 1,2,...; (b) GISP2 record (top) and cooling trends (bottom). Cooling cycles are found to culminate in Heinrich events followed by abrupt warming, causing the saw-tooth pattern described by Bond et al. (1993).

Stuiver et al. 1995; Oeschger et al. 1980). One mechanism discussed is an increase in the ocean circulation rate. The atmospheric $^{14}\text{C}/^{12}\text{C}$ value is highly sensitive to small changes in the circulation rate because the ocean contains over 65 times more carbon than the atmosphere and has a significantly lower $^{14}\text{C}/^{12}\text{C}$ ratio due to ^{14}C decay during its long residence time (Siegenthaler et al. 1980; Keir 1983). As such, an increase in the mixing rate will lower the atmospheric $^{14}\text{C}/^{12}\text{C}$ ratio to approach the oceanic value. Thus, an increase in ocean mixing during the Younger Dryas may at least be partially responsible for the atmospheric $\Delta^{14}\text{C}$ drop recorded during this time interval, although recent studies do show evidence for slowing in ocean circulation during this period (McManus et al. 2004). Alternatively, it is possible that a decrease in the ^{14}C production rate, perhaps associated with changes in the solar magnetic field (Goslar et al. 2000), may have also contributed to this drop.

Here, we examine whether there is a climatic link to the $\Delta^{14}\text{C}$ drop recorded between 15 and 14 cal kyr BP. First, we note that at least a portion of this interval corresponds to the timing of the first melt-water pulse, the most dramatic melting event during Termination I (Fairbanks 1989; Bard et al. 1990). Second, this interval corresponds to a period of generally increasing $\delta^{18}\text{O}$ in Greenland ice (cf. Figure 10b), resulting from significant temperature increases, and decreasing $\delta^{18}\text{O}$ of Chinese speleothem calcite, resulting from increases in summer Monsoon intensity (Wang et al. 2001). In addition to climatically induced carbon cycle changes, this feature could also be linked to a decrease in ^{14}C production due to changes in geomagnetic field intensity or solar activity.

We first investigate the possibility that ^{14}C production changes arising from fluctuations in the terrestrial magnetic field were the cause of the $\Delta^{14}\text{C}$ drop observed between 15 and 14 cal kyr BP. To evaluate this, we converted the SINT200 stacked paleointensity record of Guyodo and Valet (1996) into the corresponding ^{14}C production curve using the calculations of Lal (1988). Because atmospheric ^{14}C oxidizes and becomes incorporated into the larger reservoirs of the global carbon cycle, we then used the ^{14}C production data as input to a simple carbon cycle model (Houtermans and Suess 1973). The results are broadly consistent, but slightly higher than those of Beck et al. (2001) based on the SINT200 stacked geomagnetic field record and an invariant modern balanced 13-box carbon cycle. The predicted $\Delta^{14}\text{C}$ values resulting from changes in dipole shielding are shown as a dashed line in Figure 10a. Although terrestrial magnetic field changes predict a general diminution of $\Delta^{14}\text{C}$ over the interval, we find no evidence of a shift in dipole field intensity that could have produced this large, rapid $\Delta^{14}\text{C}$ drop observed in the data.

We next explore evidence that climatic shifts and associated carbon cycle changes resulted in the 15- to 14-cal kyr BP drop in $\Delta^{14}\text{C}$. In Figure 10b, we subtract out the geomagnetic contribution to the $\Delta^{14}\text{C}$ record, where the tree-ring and coral $\Delta^{14}\text{C}$ data has been combined with a 3-point moving average trendline, and compare the residual with the inverted oxygen isotope record from the Greenland Ice Sheet Project (GISP2; Grootes et al. 1997). The figure reveals a strong correlation between climate and residual $\Delta^{14}\text{C}$ changes: both the 12.5- to 11.5- and the 15- to 14-cal kyr BP intervals of falling $\Delta^{14}\text{C}$ values that create the age plateaus are associated with similar transitions in the GISP2 record. The records also hint that Greenland climate changes preceded atmospheric $\Delta^{14}\text{C}$ changes by a few hundred years. This apparent lag of atmospheric $\Delta^{14}\text{C}$ may well result from the significant residence time of carbon in the ocean. The observed correlation between climate and residual $\Delta^{14}\text{C}$ could be caused by two phenomena, either a change in ocean circulation associated with a change in climate, which changes carbon cycling and affects $\Delta^{14}\text{C}$, or a change in solar activity.

Although some solar involvement cannot be ruled out, a number of arguments suggest that the main cause of the $\Delta^{14}\text{C}$ -climate relationship is carbon cycle changes related to changes in climate. If the

$\Delta^{14}\text{C}$ changes were caused by solar changes, one would expect changes in ^{10}Be to correlate with changes in $\Delta^{14}\text{C}$ in this interval. This is indeed the case for much of the Holocene (Alley et al. 1995; Finkel and Nishiizumi 1997). However, the atmospheric/Greenland ice ^{10}Be flux is similar during the Holocene and Late Glacial (Alley et al. 1995; Finkel and Nishiizumi 1997; Hughen et al. 2000), whereas the Holocene ^{14}C fluctuations are factors of several smaller than the Late Glacial ^{14}C fluctuations considered here. Thus, unless there is large amplification of the ^{14}C response to solar variations during the Late Glacial, or there is a climatic artifact in the ice-core ^{10}Be data, it would appear that solar variation is not the main cause of the large Late Glacial $\Delta^{14}\text{C}$ shifts observed here.

The last remaining possibility, that shifts in ocean circulation caused the observed drop in $\Delta^{14}\text{C}$ recorded between 15 and 14 cal kyr BP, is difficult to evaluate directly. For example, we do not have a good understanding of paleo-ocean circulation geometry and how this may change on millennial and sub-millennial scales during deglaciation. Nevertheless, as was done for the Younger Dryas $\Delta^{14}\text{C}$ drop, we can make a qualitative argument for the 15- to 14-cal kyr BP $\Delta^{14}\text{C}$ feature. Periods of warming in Greenland observed during this interval in the GISP2 record were likely to have been accompanied by higher rates of North Atlantic Deep Water formation, and thus higher rates of ocean circulation. As discussed previously, greater ocean ventilation rates would result in a lowering in atmospheric $\Delta^{14}\text{C}$ values (cf. Stuiver et al. 1995). Thus, whereas we cannot rule out solar-related production changes, there seems to be a viable mechanism for carbon-cycle modulation of $\Delta^{14}\text{C}$ in this interval.

$\Delta^{14}\text{C}$ Excursion at 28 cal kyr BP

Figure 11 shows the new extension of the calibration between 20 and 38 cal kyr BP and the corresponding atmospheric record. Notably, 2 points with concordant ^{230}Th - ^{231}Pa ages at face value suggest a large $\Delta^{14}\text{C}$ excursion at 28 cal kyr BP. The 1100‰ offset corresponds to a ^{14}C age that is 6.8 kyr younger than the calendar age. The period prior to this peak is sparsely populated with atmospheric values hovering around 500‰, while the interval after this peak shows a clear line of descent between 700 and 400‰, in agreement with the single calibration point of Bard et al. (1990a). Including this earlier data point, the drop in atmospheric values is composed of 6 calibration points based on corals from 5 different cores drilled in Papua New Guinea, Vanuatu, and Barbados. The drop in atmospheric $\Delta^{14}\text{C}$ creates a 3000-yr age plateau in the calibration with a ^{14}C age of 19.8 ± 0.3 kyr. If confirmed, this extended ^{14}C plateau would severely complicate the use of ^{14}C dating methods to establish a chronology of events leading up to the Last Glacial Maximum.

Several aspects of the calibration data forming the ^{14}C plateau lend some support for its existence. First, the corals produce a self-consistent atmospheric history despite having originated from such diverse environments; secondly, two of the samples record concordant ^{230}Th - ^{231}Pa ages; and finally, the samples were preserved below sea level for much of their history, making them less likely to be altered. However, 2 recent studies did not show a large $\Delta^{14}\text{C}$ excursion in this time range (Hughen et al. 2004; Bard et al. 2004). These are both based on stratigraphic correlations to the GISP2 chronology and, therefore, both have inherent uncertainties associated with the accuracy of the correlations. Nevertheless, both record intermediate values for $\Delta^{14}\text{C}$ in this time interval.

If valid, the origin of the atmospheric $\Delta^{14}\text{C}$ excursion at 28 cal kyr BP is puzzling. One possibility is diagenetic inaccuracy that was not detected despite use of ^{231}Pa . Thus, it is imperative that future efforts test whether this peak can be replicated. If diagenetic inaccuracy is not the cause, there are several possible causes. One possibility is a change in cosmogenic nuclide production rates. ^{10}Be records from polar ice reveal a similar spike that is attributed to a dramatic shift in cosmogenic nuclide production rates of undetermined origin (Raisbeck et al. 1987; Yiou et al. 1997). However,

the ^{10}Be spike, thought to be the Laschamps event, occurs at roughly 40 cal kyr BP and does not match the timing of the anomaly observed here. In Figure 11a,b, shifts in the terrestrial magnetic field and resulting changes in radionuclide production rates are also examined. Modelled $\Delta^{14}\text{C}$ values resulting from changes in geomagnetic field intensity are plotted with the coral record. The plot reveals that fluctuations in paleointensity may account for 350‰ of the peak observed in the $\Delta^{14}\text{C}$ record. While the geomagnetic contribution may account for a third of the observed $\Delta^{14}\text{C}$ peak, a large portion of the $\Delta^{14}\text{C}$ excursion remains unexplained.

We again explore whether climate records provide clues of a carbon cycle change that may have triggered the observed fluctuations in the atmospheric $\Delta^{14}\text{C}$ record. As before, we plot in Figure 12 the combined tree-ring and coral data against the GISP2 oxygen isotope record, including the periods of the ^{14}C age plateaus discussed earlier. The scale of changes is very different between 10 and 20 cal kyr BP than between 20 and 35 cal kyr BP. Clearly, if the climate in Greenland and atmospheric $\Delta^{14}\text{C}$ values are linearly correlated in their response to variability in ocean circulation, the $\Delta^{14}\text{C}$ excursion could not have arisen from circulation changes alone. However, if atmospheric $\Delta^{14}\text{C}$ is linked to a different portion of the ocean system or if its response is non-linear once circulation rates pass a threshold value, then the possibility for an oceanic trigger remains open.

To further investigate the possibility of an oceanic trigger, we look to another climatic record. Figure 12b shows the GISP2 $\delta^{18}\text{O}$ profile for the last 50 kyr and the timing of “Heinrich events” 1 through 5 based on the correlation of Bond et al. (1993). Heinrich events are periods of massive ice-berg discharges from eastern Canada into the North Atlantic marked in deep-sea sediments by layers rich in ice-rafted debris and unusually poor in foraminifera (Bond et al. 1992). While the causes of these discharges remain unclear, their occurrence is linked to extreme cooling and reduced salinity of North Atlantic surface waters and the decline or suspension of North Atlantic deep-water formation and thermohaline circulation rates. Bond et al. (1993) observed that ice-core and deep-sea $\delta^{18}\text{O}$ records between 20 and 80 kyr BP exhibit matching oscillations in ocean-atmosphere temperature that are bundled into 10–15-kyr cooling cycles, each of which culminates in a Heinrich event followed by an abrupt shift to a warmer climate (Figure 12b).

Three Heinrich events occur in the GISP2 chronology between 10 and 35 cal kyr BP (Figure 12). Of the three, Heinrich event 3 (H3) occurs at about the same time as the ^{14}C peak. The period of H3 cooling may have reduced ocean circulation, bringing about increased atmospheric $\Delta^{14}\text{C}$ levels at around 30 cal kyr BP. The abrupt warming in the GISP2 record at 29 cal kyr BP may then represent a resumption in ocean ventilation rates that brought about the subsequent decline in $\Delta^{14}\text{C}$ values after 27 cal kyr BP. Although this scenario is plausible, it is not clear that the temporal relationships between the timing of H3 and the timing of the ^{14}C peak match. Furthermore, it is not clear why a ^{14}C peak associated with H3 would be much higher than that associated with other Heinrich events.

To estimate this ventilation age required to explain our peak, we first calculate the $\Delta^{14}\text{C}$ of the average ocean ($\Delta^{14}\text{C}_O$) resulting from the rise in atmospheric $\Delta^{14}\text{C}$ ($\Delta^{14}\text{C}_A$) at 30 cal kyr BP using the following steady-state equation:

$$\Delta^{14}\text{C}_O(X_O) + \Delta^{14}\text{C}_A(X_A) = \Delta^{14}\text{C}_{\text{Tot}} \quad (1),$$

where X is the fraction of carbon in each reservoir, the subscript O represents the ocean reservoir, and A the atmospheric reservoir. We can calculate the modern values of $\Delta^{14}\text{C}_{\text{Tot}}$ from our knowledge of the present values of all of the variables above. We then presume a value for $\Delta^{14}\text{C}_{\text{Tot}}$ at the time of the peak of 1.35 times the modern value, accounting for the 350‰ elevation in $\Delta^{14}\text{C}$ due to reduced magnetic shielding (see above). Assuming modern values for the fraction of carbon in the atmos-

pheric and oceanic reservoirs and 1100‰ for $\Delta^{14}\text{C}_A$, we calculate a value of 162‰ for $\Delta^{14}\text{C}_O$ at the time of the peak compared to the present-day value of -130‰.

The ventilation age (t) is then determined using the following relationship:

$$t = 8033 \ln [^{14}\text{C}/^{12}\text{C}_{\text{atmosphere}} / ^{14}\text{C}/^{12}\text{C}_{\text{ocean}}] \quad (2),$$

where 8033 is the mean life of ¹⁴C based on the Libby half-life. We find that the ventilation age would have been roughly 4800 yr if a reduction in ocean circulation produced the excursion observed in the coral $\Delta^{14}\text{C}$ record. This is on the order of 4 times the modern value and is calculated on a steady-state basis. A non-steady-state calculation would likely require even larger ventilation age. One could question the plausibility of this explanation and the plausibility of this high of an atmospheric ¹⁴C value. Therefore, we encourage attempts to test our data with samples from other sites. There is, however, at present some independent data that is at least consistent with our ¹⁴C peak. Sikes et al. (2000) show large apparent differences between atmospheric and oceanic $\Delta^{14}\text{C}$ near New Zealand at about the time of our ¹⁴C peak. If, in fact, these data can be confirmed, they could either be interpreted as resulting from a large oceanic ventilation age (as inferred by Sikes et al. 2000; of the same magnitude as our calculated value), or as a result of rapidly rising atmospheric $\Delta^{14}\text{C}$ or both. The latter possibility is related to an effect pointed out by Adkins and Boyle (1997). If atmospheric ¹⁴C rises during the interval between deep-water formation and deep-water aging, then the difference between atmospheric ¹⁴C and deep-water ¹⁴C subsequent to the aging process will yield an apparent age that is larger than the true age of the deep water. If this is, in part, the explanation of the Sikes et al. (2000) data, then this would support the idea of rapidly falling atmospheric ¹⁴C subsequent to the 28-kyr peak. If high ventilation age is, in part, the explanation of the Sikes et al. (2000) data, then this would support the high ventilation age explanation of our 28-kyr peak. Nevertheless, we emphasize the need to test both the Sikes et al. (2000) work and our apparent 28-kyr peak. If our peak is indeed accurate, it is likely that both low terrestrial magnetic field values and slower oceanic circulation rates contributed to the high ¹⁴C values.

Marine $\delta^{234}\text{U}$

Figure 4 reveals that the majority of analyses fall within 8‰ of the modern marine value (hatched box). However, within these narrow bounds, there appears to be a slight trend in $\delta^{234}\text{U}_i$ values. The open box delineates the $\delta^{234}\text{U}_i$ bounds of 17 Papua New Guinea drill core samples analyzed by Edwards et al. (1993). The $\delta^{234}\text{U}_i$ value of each of these samples was indistinguishable, with a precision of $\pm 1\%$ of the modern marine value, and no age reversals were found down core. The strong internal consistency of this data set and agreement with the modern marine value suggests that these samples are unaltered and the bounds of this box represent the marine $\delta^{234}\text{U}$ value, with a precision of $\pm 2\%$, during that period. Using this box as a reference then, the plot shows a possible shift, an increase of as much as 6‰ in the marine $\delta^{234}\text{U}$ value, between 22 and 12 cal kyr BP. This period includes the first half of the last deglaciation. Note that Esat et al. (2000) and Henderson et al. (2002) have documented low $\delta^{234}\text{U}$ values during the last glacial period and that a number of studies (Edwards 1988; Hamelin et al. 1991; Richter and Turekian 1993; Esat et al. 2000; Henderson et al. 2002; Edwards et al. 2003; Robinson et al. 2003) explore the causes of possible marine $\delta^{234}\text{U}$ shifts. We explore the possible causes of such as shift below.

In Figure 13, we plot the $\delta^{234}\text{U}_i$ values of samples with ²³⁰Th-²³¹Pa concordant ages to evaluate whether the observed trend in Figure 4 is a product of coral diagenesis or due to a real shift in the marine $\delta^{234}\text{U}$ value. The samples, from Cutler et al. (2003), Edwards et al. (1997), and this work, originate from Papua New Guinea and range in age from 9 to 93 cal kyr BP. Similar to Figure 4, the

data in Figure 13 indicate that the marine $\delta^{234}\text{U}$ value has remained constant within about 8‰ over the last 95 kyr. In addition, it also supports a possible small rise in the marine $\delta^{234}\text{U}$ value during the early portion of deglaciation. The timing of this possible rise is an issue. Figure 13 shows that seawater $\delta^{234}\text{U}$ has been within 2‰ of its present value for the last 12 kyr, and was generally about 6‰ lower than this value from ~60 kyr BP to ~22 kyr BP. There is some discrepancy in values at ~25 kyr BP, as there are 2 relatively high values at this time. However, as the bulk of the values during this interval are low, we presume the marine value was low at this time. Therefore, we now consider possible explanations for a rise in marine $\delta^{234}\text{U}$ between 22 and 12 kyr BP.

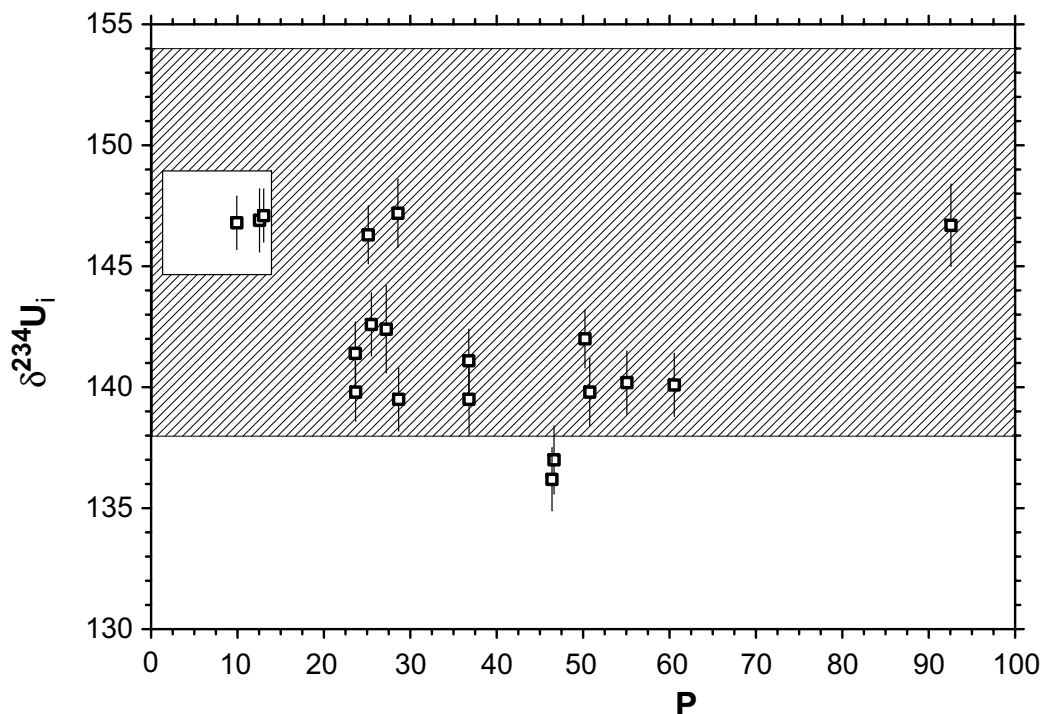


Figure 13 $\delta^{234}\text{U}_i$ versus age diagram for samples with concordant ^{230}Th - ^{231}Pa ages. Hatched and open envelopes are same as Figure 4. Square symbols are $\delta^{234}\text{U}_i$ data for ^{230}Th - ^{231}Pa age-concordant samples from Papua New Guinea and are from Cutler et al. (2003), Edwards et al. (1997), and this study. Replicate analyses are included; error bars are 2σ .

While further studies will be needed to confirm this shift as a marine phenomenon, these observations raise the question of whether a several per mil shift in the marine uranium isotopic composition is possible over these time scales. Ku et al. (1977) obtained a residence time for uranium in the ocean between 200,000 and 400,000 yr, which places strong limits on the rate of change in the marine $^{234}\text{U}/^{238}\text{U}$ value (Edwards 1988; Hamelin et al. 1991; Richter and Turekian 1993; Henderson et al. 2002). To explore whether a several per mil shift in marine $\delta^{234}\text{U}$ during the early portion of deglaciation was possible, we consider 3 mechanisms.

Our first mechanism is based on the findings of Russell et al. (1994). Here, the authors suggest that the uranium concentration in seawater shifts with the glacial-interglacial cycles due to increased productivity and reduced oxygen content in seawater during glacial times. Because the reduced form of uranium adsorbs more easily onto sediments and settles out of the water column, the authors speculate that the average U concentration in seawater may have been lower during glacial periods. Dur-

ing interglacial times, they suggest that the average U concentration in seawater is higher because it is no longer being tied up in the sediment. Inflowing riverine ²³⁴U remains in solution and ²³⁴U tied up in the sediment becomes oxidized and soluble. The seawater $\delta^{234}\text{U}$, however, would decrease during this glacial to interglacial transition, because the average $\delta^{234}\text{U}$ value of the sediment would have decreased through time due to radioactive decay of ²³⁴U. As such, this mechanism does not support the sign of the observed shift in the marine $\delta^{234}\text{U}$ value derived from the coral data.

For the second mechanism, we examine the likelihood that a change in riverine $\delta^{234}\text{U}$ may have produced the observed shift in marine $\delta^{234}\text{U}$ values. Modern rivers have $\delta^{234}\text{U}$ values that range between 100 and 500‰ (Ivanovich and Harmon 1982) and have an average value of about 270‰. The spread in values arises from differences in isotopic composition and concentration of source rocks, as well as variability in erosion rates and processes.

Edwards (1988) calculated how marine $\delta^{234}\text{U}$ would change due to an instantaneous shift in riverine $\delta^{234}\text{U}$. He envisioned an ocean at steady-state with regard to ²³⁸U and initially at steady-state with regard to $\delta^{234}\text{U}$, and that the only uranium source is riverine. At $t = 0$, the system is perturbed by a shift in average riverine $\delta^{234}\text{U}$; the flux of ²³⁸U is assumed to remain constant. Based on these conditions, Edwards calculated that for times short compared to the residence time of U in the oceans and the mean life of ²³⁴U (353 kyr), that the response of the ocean to this perturbation is approximated by

$$\Delta\delta_r = \Delta\delta_m (\tau_U/t) \tag{3}$$

where t is the time over which the change occurs, τ_U is the residence time of uranium in the ocean, and the riverine flux and marine uranium concentration are assumed constant. If $\Delta\delta_m$ is set equal to 6‰, t to 10,000 yr, and τ_U to 300,000 yr, we find that an increase in the average riverine $\delta^{234}\text{U}$ value of 180‰, or 45% of its range, is required to produce the shift observed between 22 and 12 cal kyr BP. This is a large but plausible shift in riverine $\delta^{234}\text{U}$. Robinson et al. (2003) have recently shown that streams draining glaciated areas in New Zealand have extremely high $\delta^{234}\text{U}$ values approaching 4000‰. Thus, it is plausible that the average riverine $\delta^{234}\text{U}$ could have risen by large amounts. The time frame of the shift and the new Robinson et al. data point to one possible mechanism for its occurrence. With the retreat of the ice sheets, formerly glaciated areas became exposed to erosion. Because ²³⁴U sites in the crystal lattice are damaged during the decay of ²³⁸U to ²³⁴U, ²³⁴U is preferentially leached from the rock structure (Ivanovich and Harmon 1982). As a result, rocks freshly exposed to weathering might yield higher $\delta^{234}\text{U}$ values than previously eroded surfaces.

For the third mechanism, we explore the possibility that a shift in the riverine uranium flux into the ocean may have been responsible for the observed shift in the marine isotopic composition. At steady-state, this flux, dU/dt , is related to the uranium residence time in the ocean by the equation

$$dU/dt = U/\tau_U \tag{4}$$

where U is the total amount of uranium in the ocean. We calculate, then, the change in τ_U required to produce the observed shift in the coral record using a similar model (Edwards 1988) to the one above. To do this, we assume that the riverine $\delta^{234}\text{U}$ value and marine uranium concentration remain constant and that the initial marine $\delta^{234}\text{U}$ value (δ_m^0) is at steady-state (*ss*). At $t = 0$, the riverine U flux changes instantaneously, causing the marine isotopic composition to approach a new steady-state value (δ_m^1) as described by the equation

$$\delta_m = \delta_m^1(ss) + [\delta_m^0(ss) - \delta_m^1(ss)] [\exp(-(1/\tau_U + 1/\tau_{234})t)] \tag{5}$$

where δ_m is the marine isotopic value at time t , τ_{234} is the mean life of ^{234}U (353 kyr), and τ_U is equal to $U/(dU/dt)$ after the change in U flux.

The equation shows that the marine isotopic composition changes from its initial steady-state value to its new steady-state value with a time constant of $1/\tau_U + 1/\tau_{234}$, and has a value of δ_m after t yr. The new steady-state value is defined as

$$\delta_m^1(ss) = \delta_r / (1 + \tau_U / \tau_{234}) \quad (6).$$

If δ_m^0 is set equal to 140‰, δ_m to 146‰, and t to 10,000 yr, equations (5) and (6) can be simultaneously solved. We find that during deglaciation, the ocean residence time had to increase by a factor of 2.4, from 125 kyr to its present-day value of 300 kyr, to produce the 6‰ change observed in the coral $\delta^{234}\text{U}$ record. Inversely, the riverine flux of uranium had to decrease by a factor of 2.4 to produce this change. Although it is likely that riverine uranium fluxes change to some degree on glacial to interglacial time scales, there is no other evidence suggesting a change of that magnitude.

Of the 3 mechanisms examined, we find that the second mechanism, based on a rise in riverine $\delta^{234}\text{U}$, is best able to explain the 6‰ observed increase in the marine $\delta^{234}\text{U}$ value between 22 and 12 cal kyr BP. This mechanism calls for an increase in the average riverine $\delta^{234}\text{U}$ value of 180‰, or 45% of its range. This large shift in riverine $\delta^{234}\text{U}$ is plausible given that the retreating ice sheets were freshly exposing large areas to weathering that likely yielded higher $\delta^{234}\text{U}$ values than previously eroded surfaces (see Robinson et al. 2003). Some combination of a rise in riverine $\delta^{234}\text{U}$ and a decrease in riverine uranium flux (the third mechanism) may also explain the observed trend in marine $\delta^{234}\text{U}$. We emphasize that this possible shift in marine $\delta^{234}\text{U}$ should be verified with additional careful studies that employ ^{231}Pa dating to test for concordancy.

CONCLUSIONS

The new calibration data map ^{14}C variations from the current extent of the tree-ring calibration, 11.9 cal kyr BP, to the ^{14}C dating limit of 50 cal kyr BP. The data reveal that the gradually widening gap between the calibrated and ^{14}C ages observed in the younger portions of the calibration continues to increase with age until 28 cal kyr BP, when the ^{14}C age is 6800 yr too young. The coral calibration points prior to 28 cal kyr BP indicate less of a gap between the calibrated and ^{14}C age of between 4000 to 5000 yr.

Significantly, the new data reveals 2 previously unidentified ^{14}C age plateaus between 14 and 15 cal kyr BP and between 22 and 25 cal kyr BP. The plateaus correspond to ^{14}C ages of 12.4 ± 0.2 kyr and 19.8 ± 0.3 kyr, respectively, and limit ^{14}C dating resolution for their duration. While the origin of these plateaus remains somewhat in question, we found that changes in carbon cycling are likely the source of the younger plateau and a large contributing factor to the older plateau.

For the younger plateau, we found a strong correlation between climate—as revealed in the Greenland oxygen isotope record—and changes in residual $\Delta^{14}\text{C}$ values, when the contribution from geomagnetic field changes was subtracted out. This correlation can be explained by the probable causal relationships between periods of warming in Greenland, higher rates of ice sheet melting, North Atlantic Deep Water formation and ocean circulation, and decreasing values in atmospheric $\Delta^{14}\text{C}$.

The origins of the older plateau are not as clear, but may also be linked to abrupt slowing in ocean circulation rates, combined with the effects of terrestrial magnetic field fluctuations. Evidence for this comes from the Greenland ice-core records and records of severe cooling, called Heinrich events. Heinrich event 3, which is distinct in its long duration, lower $\delta^{18}\text{O}$ values, and extreme shifts in temperature, takes place just prior to the peak in atmospheric $\Delta^{14}\text{C}$ values. The extended period

of H3 cooling may have reduced ocean circulation, bringing about a rapid escalation in atmospheric $\Delta^{14}\text{C}$ levels observed at 30 cal kyr BP. The abrupt warming in the Greenland ice-core record at 29 cal kyr BP may then represent a resumption in ocean ventilation rates that brought about the subsequent decline in $\Delta^{14}\text{C}$ values after 27 cal kyr BP. These fluctuations alone, however, do not provide a full explanation for this pronounced peak, and future studies should aim to test whether or not our peak may relate to diagenetic shifts in age or ^{14}C content.

Finally, we found evidence of a possible 6‰ increase in the marine $\delta^{234}\text{U}$ value during the early portion of deglaciation, between 22 and 12 cal kyr BP. While the presence for such a shift requires further study, we examined whether a several per mil shift in the marine uranium isotopic composition is possible over these time scales. We found that a rise in average riverine $\delta^{234}\text{U}$ of 180‰, or 45% of its range, is best able to explain the observed increase in the marine $\delta^{234}\text{U}$ value. This large shift in riverine $\delta^{234}\text{U}$ is plausible given that the retreating ice sheets were freshly exposing large areas to weathering that likely yielded higher $\delta^{234}\text{U}$ values than previously eroded surfaces.

ACKNOWLEDGMENTS

We thank the many local people in Vanuatu and Papua New Guinea that helped with this work, John Chappell and Eugene Wallenski for help in drilling in Papua New Guinea, Jacques Recy for help in drilling in Vanuatu, and G R Min who helped with field work in Papua New Guinea. This work was supported by NSF grants 971203, 9809459, 0116395, 0223239, 0402249, and 9809459 to R L E.

REFERENCES

- Adkins J, Boyle EA. 1997. Changing atmospheric $\Delta^{14}\text{C}$ and the record of deep-water paleoventilation ages. *Paleoceanography* 12:337–44.
- Alley RB, Finkel RC, Nishiizumi K, Anandkrishnan S, Shuman CA, Mershon GR, Zielinski GA, Mayewski PA. 1995. Changes in continental and sea-salt atmospheric loadings in central Greenland during the most recent deglaciation: model-based estimates. *Journal of Glaciology* 41:503–14.
- Andree M, Oeschger H, Broecker W, Beavan N, Klas M, Bonani G, Hofmann HJ, Suter M, Wöflfi W, Peng T-H. 1986. Limits on the ventilation rate for the deep ocean over the last 12,000 years. *Climate Dynamics* 1:53–62.
- Bard E, Hamelin B, Fairbanks RG, Zindler A. 1990. Calibration of the ^{14}C time scale over the past 30,000 years using mass spectrometric U-Th ages from Barbados corals. *Nature* 345:405–10.
- Bard E, Arnold M, Fairbanks RG, Hamelin B. 1993. ^{230}Th - ^{234}U and ^{14}C ages obtained by mass spectrometry on corals. *Radiocarbon* 35(1):191–9.
- Bard E, Hamelin B, Arnold M, Montaggioni L, Cabioch G, Faure G, Rougerie F. 1996. Deglacial sea-level record from Tahiti corals and the timing of global meltwater discharge. *Nature* 382:241–4.
- Bard E, Arnold M, Hamelin B, Tisnerat-Laborde N, Cabioch G. 1998. Radiocarbon calibration by means of mass spectrometric $^{230}\text{Th}/^{234}\text{U}$ and ^{14}C ages of corals: an updated database including samples from Barbados, Mururoa and Tahiti. *Radiocarbon* 40(3):1085–92.
- Bard E, Rostek F, Ménot-Combes G. 2004. Radiocarbon calibration beyond 20,000 ^{14}C yr BP by means of planktonic foraminifera of the Iberian Margin. *Quaternary Research* 61:204–14.
- Beck JW, Richards DA, Edwards RL, Silverman BW, Smart PL, Donahue DJ, Hererra-Osterheld S, Burr GS, Calsoyas L, Jull AJT, Biddulph D. 2001. Extremely large variations of atmospheric ^{14}C concentration during the last glacial period. *Science* 292:2453–8.
- Bond G, Heinrich H, Broecker W, Labeyrie L, McManus J, Andrews J, Huon S, Jantschik R, Clasen S, Simet C, Tedesco K, Klas M, Bonani G, Ivy S. 1992. Evidence for massive discharges of icebergs into the North Atlantic Ocean during the last glacial period. *Nature* 360:245–9.
- Bond G, Broecker W, Johnsen S, McManus J, Labeyrie L, Jouzel J, Bonani G. 1993. Correlations between climate records from North Atlantic sediments and Greenland ice. *Nature* 365:143–7.
- Burr GS, Edwards RL, Donahue DJ, Druffel ERM, Taylor FW. 1992. Mass spectrometric ^{14}C and U-Th measurements in coral. *Radiocarbon* 34(3):611–8.
- Burr GS, Beck JW, Taylor FW, Recy J, Edwards RL, Cabioch G, Corregge T, Donahue DJ, O'Malley JM. 1998. A high-resolution radiocarbon calibration between 11,700 and 12,400 calendar years BP derived from ^{230}Th ages of corals from Espiritu Santo Island, Vanuatu. *Radiocarbon* 40(3):1093–105.
- Chappell J, Polach H. 1991. Post-glacial sea-level rise from a coral record at Huon Peninsula, Papua New Guinea. *Nature* 349:147–9.
- Cheng H, Edwards RL, Hoff J, Gallup CD, Richards DA, Asmerom Y. 2000. The half-lives of uranium-234 and thorium-230. *Chemical Geology* 169:17–33.

- Cheng H, Edwards RL, Murrell MT, Benjamin TM. Uranium-thorium-protactinium dating systematics. *Geochimica et Cosmochimica Acta* 62:3457–62.
- Cutler KB, Edwards RL, Taylor FW, Cheng H, Adkins J, Gallup CD, Cutler PM, Burr GS, Chappell J, Bloom AL. 2003. Rapid sea-level fall and deep ocean temperature change since the last interglacial period. *Earth and Planetary Science Letters* 206:253–71.
- Edwards RL, Chen JH, Wasserburg GJ. 1987a. ^{238}U - ^{234}U - ^{230}Th - ^{232}Th systematics and the precise measurement of time over the past 500,000 years. *Earth and Planetary Science Letters* 81:175–92.
- Edwards RL, Chen JH, Ku TL, Wasserburg GJ. 1987b. Precise timing of the last interglacial period from mass spectrometric determination of ^{230}Th in corals. *Science* 236:1547–53.
- Edwards RL. 1988. *High Precision ^{230}Th Thorium Ages of Corals and the Timing of Sea Level Fluctuations in the Late Quaternary*. Pasadena: California Institute of Technology.
- Edwards RL, Beck JW, Burr GS, Donahue DJ, Chappell JMA, Bloom AL, Druffel ERM, Taylor FW. 1993. A large drop in atmospheric $^{14}\text{C}/^{12}\text{C}$ and reduced melting in the Younger Dryas, documented with ^{230}Th ages of corals. *Science* 260:962–8.
- Edwards RL, Cheng H, Murrell MT, Goldstein SJ. 1997. Protactinium-231 dating of carbonates by thermal ionization mass spectrometry: implications for Quaternary climate change. *Science* 276:782–6.
- Edwards RL, Gallup CD, Cheng H. 2003. Uranium-series dating of marine and lacustrine carbonates. In: Bourdon B, Henderson G, Lundstrom C, Turner S, editors. *Reviews in Mineralogy and Geochemistry v52: Uranium-Series Geochemistry, Chapter 9*. Washington, DC: Mineralogical Society of America. p 363–406.
- Esat TM, Yokoyama Y. 2000. Correlated uranium and sea-level fluctuations in late Quaternary oceans. Goldschmidt Conference, September 3–8, Oxford, United Kingdom. *Journal of Conference Abstracts* v.5(2): 387.
- Fairbanks RG. 1989. A 17,000-year glacio-eustatic sea level record: influence of glacial melting rates on the Younger Dryas event and deep-ocean circulation. *Nature* 342:637–42.
- Finkel RC, Nishiizumi J. 1997. ^{10}Be concentration in the Greenland Ice Sheet Project 2 Ice Core from 3 to 40 ka. *Journal of Geophysical Research* 102:699–706.
- Galewskyr J, Silver EA, Gallup CD, Edwards RL, Potts DC. 1996. Foredeep tectonics and carbonate platform dynamics in the Huon Gulf, Papua New Guinea. *Geology* 24:819–22.
- Gallup CD, Edwards RL, Johnson RG. 1994. The timing of high sea levels over the past 200,000 years. *Science* 263:796–800.
- Genty D, Massault M, Gilmour M, Baker A, Verheyden S, Kepens E. 1999. Calculation of past dead carbon proportion and variability by the comparison of AMS ^{14}C and TIMS U/Th ages on two holocene stalagmites. *Radiocarbon* 41(3):251–70.
- Geyh MA, Schluchter C. 1998. Calibration of the ^{14}C time scale beyond 22,000 BP. *Radiocarbon* 40(1): 475–82.
- Goslar T, Arnold M, Bard E, Kuc T, Pazdur MF, Ralska-Jasiewiczowa M, Rozanski K, Tisnerat N, Walanus A, Wicik B, Wieckowski K. 1995. High concentration of atmospheric ^{14}C during the Younger Dryas cold episode. *Nature* 377:414–7.
- Goslar T, Arnold M, Tisnerat-Laborde N, Czernik J, Wieckowski K. 2000. Variations of Younger Dryas atmospheric radiocarbon explicable without ocean circulation changes. *Nature* 403:877–80.
- Grootes PM, Stuiver M. 1997. Oxygen-18/16 variability in Greenland snow and ice with 10^3 to 10^5 -year time resolution. *Journal of Geophysical Research* 102: 26,455–70.
- Guyodo Y, Valet J-P. 1996. Relative variations in geomagnetic intensity from sedimentary records: the past 200,000 years. *Earth and Planetary Science Letters* 143:23–36.
- Hajdas I, Ivy SD, Beer J, Bonani G, Imboden D, Lotter AF, Sturm M, Suter M. 1993. AMS radiocarbon dating and varve chronology of Lake Soppensee: 6000 to 12,000 ^{14}C years BP. *Climate Dynamics* 9:107–16.
- Hajdas I, Zolitschka B, Ivy-Ochs SD, Beer J, Bonani G, Leroy SAG, Negendank JW, Ramrath M, Suter M. 1995. AMS radiocarbon dating of annually laminated sediments from Lake Holzmaar, Germany. *Quaternary Science Reviews* 14:137–43.
- Hamelin B, Bard E, Zindler A, Fairbanks RG. 1991. $^{234}\text{U}/^{238}\text{U}$ mass spectrometry of corals: How accurate is the U-Th age of the last interglacial period? *Earth and Planetary Science Letters* 106:169–80.
- Henderson GM. 2002. Seawater $^{234}\text{U}/^{238}\text{U}$ during the last 800,000 years. *Earth and Planetary Science Letters* 199:97–110.
- Houtermans JC, Suess HE. 1973. Reservoir models and production rate variations of natural radiocarbon. *Journal of Geophysical Research* 78:1897.
- Hughen KA, Overpeck JT, Lehman SJ, Kashgarian M, Southon J, Peterson LC, Alley R, Sigman DM. 1998. Deglacial changes in ocean circulation from an extended radiocarbon calibration. *Nature* 391:65–8.
- Hughen KA, Southon JR, Lehman SJ, Overpeck JT. 2000. Synchronous radiocarbon and climate shifts during the last deglaciation. *Science* 290:1951–4.
- Hughen K, Lehman S, Southon J, Overpeck J, Marchal O, Herring C, Turnbull J. 2004. ^{14}C activity and global carbon cycle changes over the past 50,000 years. *Science* 303:202–7.
- Ivanovich M, Harmon RS, editors. *Uranium Series Disequilibrium: Applications to Environmental Problems*. Oxford: Clarendon.
- Keir RS. 1983. Reduction of thermohaline circulation during the deglaciation: the effect on atmospheric radiocarbon and CO_2 . *Earth and Planetary Science Letters* 64:445–56.

- Kitagawa H, van der Plicht J. 1998. Atmospheric radiocarbon calibration to 45,000 yr BP: Late Glacial fluctuations and cosmogenic isotope production. *Science* 279:1187–90.
- Kromer B, Spurk M. 1988. Revision and tentative extension of the tree-ring based ¹⁴C calibration, 9200–11,855 cal BP. *Radiocarbon* 40(3):1117–25.
- Ku TL, Knauss KG, Mathieu GG. 1977. Uranium in the open ocean: concentration and isotopic composition. *Deep-Sea Research* 24:1005–17.
- Lal D. 1988. Theoretically expected variations in the terrestrial cosmic-ray production rates of isotopes. In: Corso XCV, editor. *Solar-Terrestrial Relationships and the Earth Environment in the Last Millennia. Societa Italiana di Fisica* 95:216–33.
- Libby WF. 1955. *Radiocarbon Dating*. Chicago: University of Chicago Press.
- McManus JF, Francois R, Gherardi J-M, Keigwin LD, Brown-Leger S. 2004. Collapse and rapid resumption of Atlantic meridional circulation linked to deglacial climate changes. *Nature* 428:834–7.
- Oeschger H, Welten M, Eicher U, Möll M, Riesen T, Siegenthaler U, Wegmüller S. 1980. ¹⁴C and other parameters during the Younger Dryas cold phase. *Radiocarbon* 22(2):299–310.
- Ota Y, Chappell J, Kelley R, Yonekura N, Matsumoto E, Nishimura T, Head J. 1993. Holocene coral reef terraces and coseismic uplift of Huon Peninsula, Papua New Guinea. *Quaternary Research* 40:177–88.
- Pickett DA, Murrell MT, Williams RW. 1994. Determination of femtogram quantities of protactinium in geologic samples by thermal ionization mass spectrometry. *Analytical Chemistry* 66:1044–9.
- Raisbeck GM, Yiou F, Bourles D, Lortius C, Jouzel J, Barkov NI. 1987. Evidence for two intervals of enhanced ¹⁰Be deposition in Antarctic ice during the last glacial period. *Nature* 326:273–7.
- Richter FM, Turekian KK. 1993. Simple models for the geochemical response of the ocean to climatic and tectonic forcing. *Earth and Planetary Science Letters* 119:121–31.
- Robert J, Miranda CF, Muxart R. 1969. Mesure de la periode du protactinium-231 par microcalorimetrie. *Radiochimica Acta* 50:104–8.
- Robinson LS, Henderson GM, Hall L, Matthews I. 2003. Controls on $\delta^{234}\text{U}$ in surface waters of the South Island, New Zealand. *EOS Transactions, AGU* v.84(46):Fall Meeting Supplement. Abstract v51c-0306.
- Russell AD, Emerson S, Nelson BK, Erez J, Lea DW. 1994. Uranium in foraminiferal calcite as a recorder of seawater uranium concentrations. *Geochimica et Cosmochimica Acta* 58:671–81.
- Schramm A, Stein M, Goldstein SL. 2000. Calibration of the ¹⁴C time scale to >40 ka by ²³⁴U-²³⁰Th dating of Lake Lisan sediments (last glacial Dead Sea). *Earth and Planetary Science Letters* 175:27–40.
- Shen CC, Cheng H, Edwards RL, Bradley Moran S, Edmonds HN, Hoff JA, Thomas RB. 2003. Measurement of attogram quantities of ²³¹Pa in dissolved and particulate fractions of seawater by isotope dilution thermal ionization mass spectroscopy. *Analytical Chemistry* 75:1075–9.
- Siegenthaler U, Heimann M, Oeschger H. 1980. ¹⁴C variations caused by changes in the global carbon cycle. *Radiocarbon* 22(2):177–91.
- Sikes EL, Samson CR, Guilderson TP, Howard WR. 2000. Old radiocarbon ages in the southwest Pacific Ocean during the last glacial period and deglaciation. *Nature* 405:555–9.
- Stein M, Wasserburg GJ, Aharon P, Chen JH, Zhu ZR, Bloom A, Chappell J. 1993. TIMS U-series dating and stable isotopes of the last interglacial event in Papua New Guinea. *Geochimica et Cosmochimica Acta* 57:2541–54.
- Stuiver M. 1978. Radiocarbon time scale tested against magnetic and other dating methods. *Nature* 273:271–4.
- Stuiver M, Grootes PM, Braziunas TF. 1995. The GISP2 $\delta^{18}\text{O}$ record of the past 16,500 years and the role of the sun, ocean, and volcanoes. *Quaternary Research* 44:341–54.
- Stuiver M, Reimer PJ, Bard E, Beck JW, Burr GS, Hughen KA, Kromer B, McCormac G, van der Plicht J, Spurk M. 1998. IntCal98 radiocarbon age calibration, 24,000–0 cal BP. *Radiocarbon* 40(3):1041–83.
- Suess HE. 1970. The three causes of the secular ¹⁴C fluctuations, their amplitudes and time constants. *Proceedings XII Nobel Symposium*. New York: Wiley. p 569–606.
- Tauber H. 1970. *The Scandinavian Varve Chronology and ¹⁴C Dating in Radiocarbon Variations and Absolute Chronology* [Olsson IU, editor]. New York: Wiley and Sons. p 173–96.
- Taylor FW, Bevis MG, Edwards RL, Gray S, Cutler KB, Phillips DA, Cabioch G, Mann P. Forthcoming. Alternating rapid forearc subsidence and uplift caused by impinging bathymetric features: examples from the New Hebrides and Solomon Arcs. *Journal of Geophysical Research*.
- van Kreveld S, Sarnthein M, Erlenkeuser H, Grootes P, Jung S, Nadeau MJ, Pflaumann U, Voelker A. 2000. Potential links between surging ice sheets, circulation changes, and the Dansgaard-Oeschger cycles in the Irminger Sea, 60–18 kyr. *Paleoceanography* 15:425–42.
- Voelker AHL, Sarnthein M, Grootes PM, Erlenkeuser H, Laj C, Mazaud A, Nadeau M-J, Schleicher M. 1998. Correlation of marine ¹⁴C ages from the Nordic Seas with the GISP2 isotope record: implications for ¹⁴C calibration beyond 25 ka BP. *Radiocarbon* 40(1):517–34.
- Vogel JC, Kronfeld J. 1998. Calibration of radiocarbon dates for the Late Pleistocene using U/Th dates on stalagmites. *Radiocarbon* 40(1):27–32.
- Yiou F, Raisbeck GM, Baumgartner SM, Beer J, Hammer CU, Johnsen SJ, Jouzel J, Kubik PW, Lestringuez J, Stiévenard M, Suter M, Yiou P. 1997. ¹⁰Be in the GRIP ice core at Summit, Greenland. *Journal of Geophysical Research* 102:26,783–94.

APPENDIX

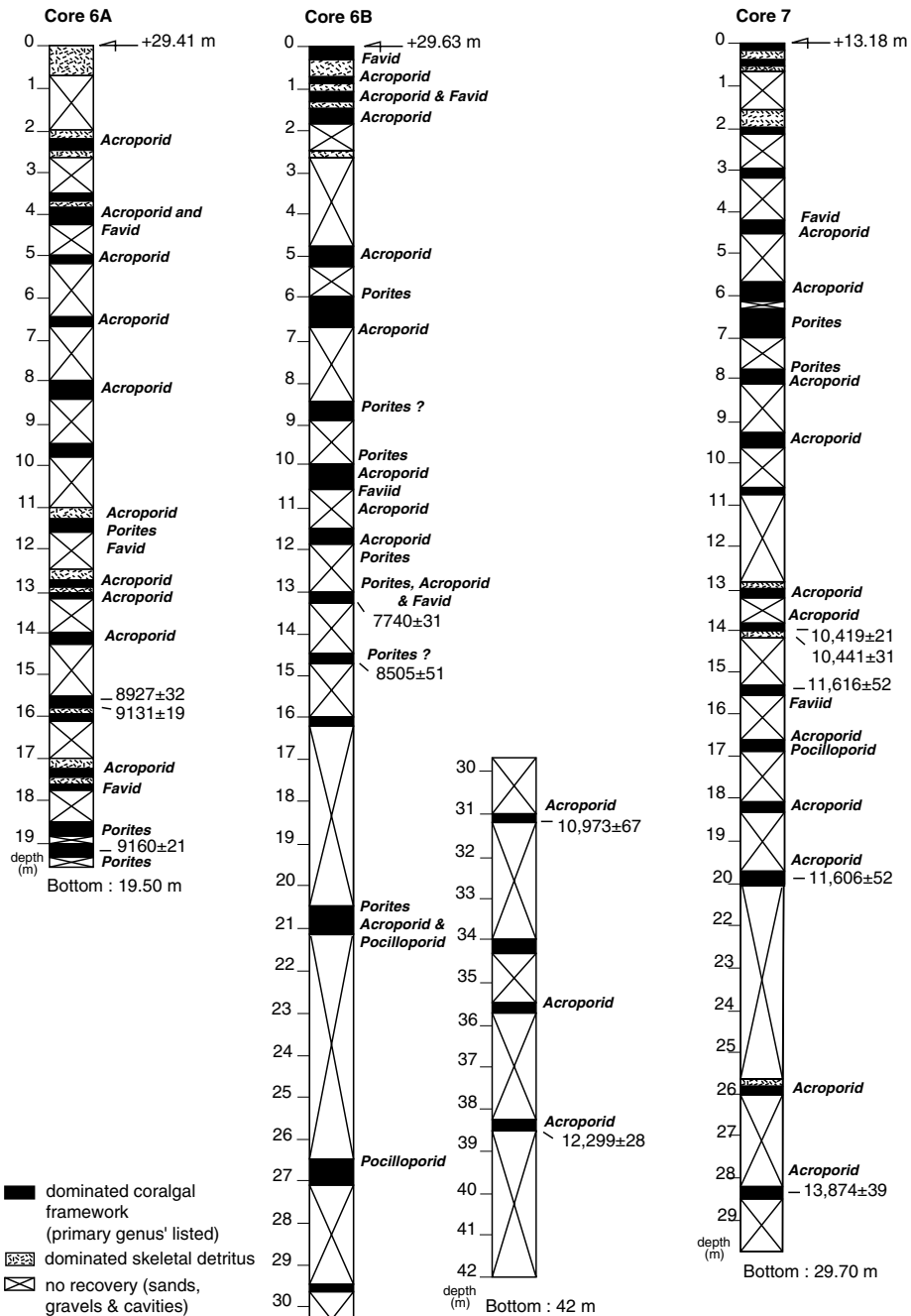


Figure 14 Vanuatu core logs 6A, 6B, and 7

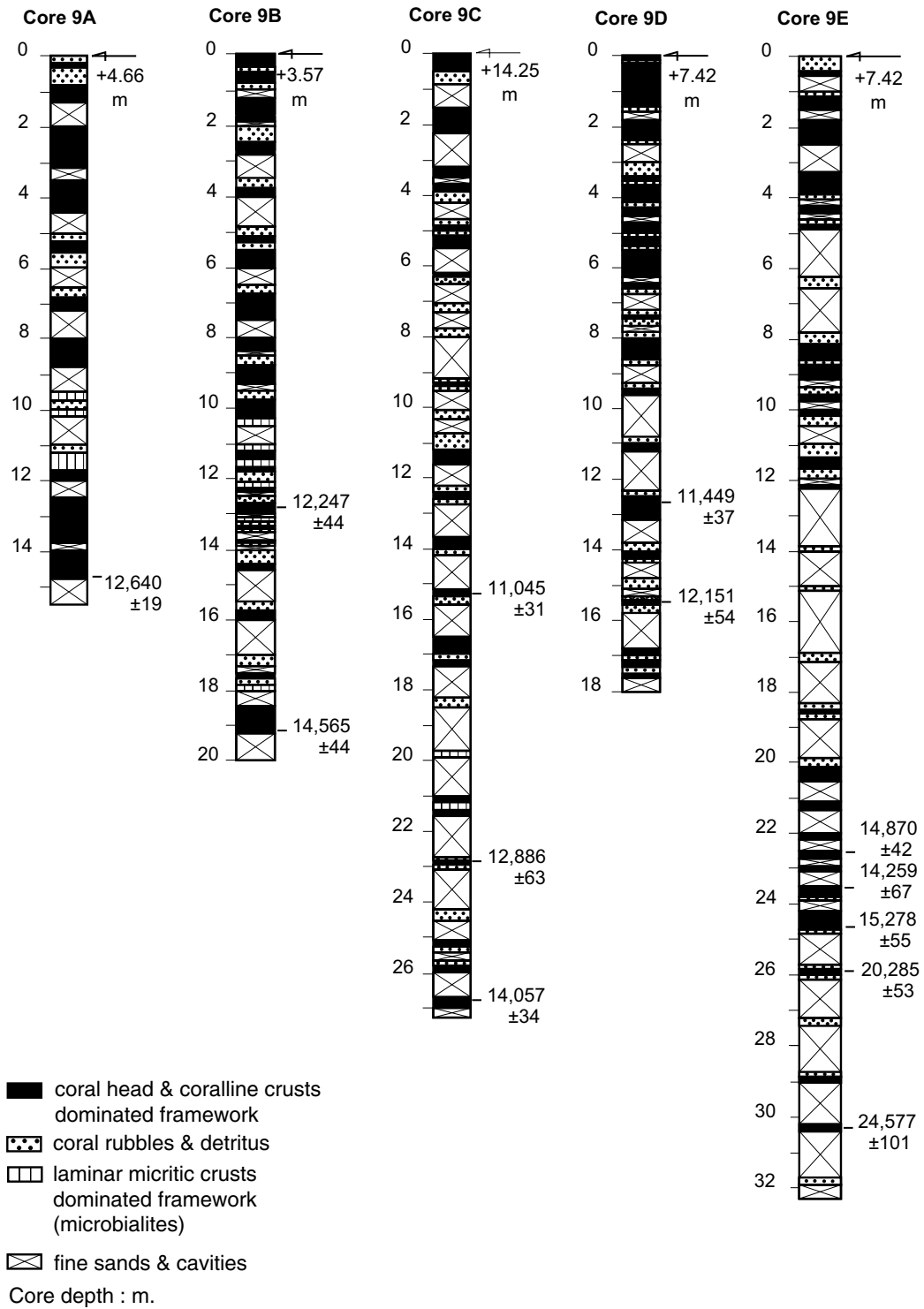


Figure 15 Vanuatu core logs 9A–E

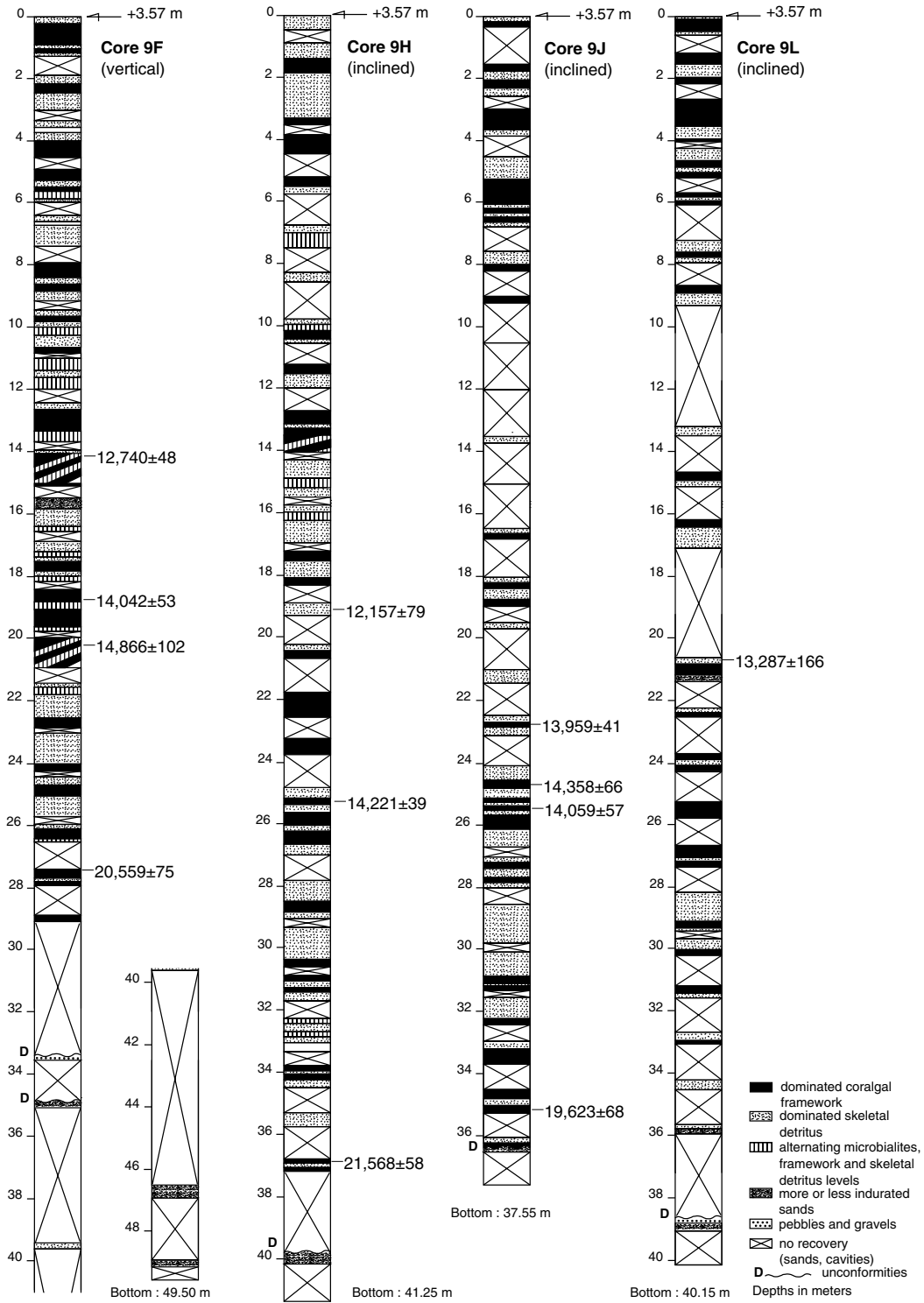


Figure 16 Vanuatu core logs 9F, H, J, and L

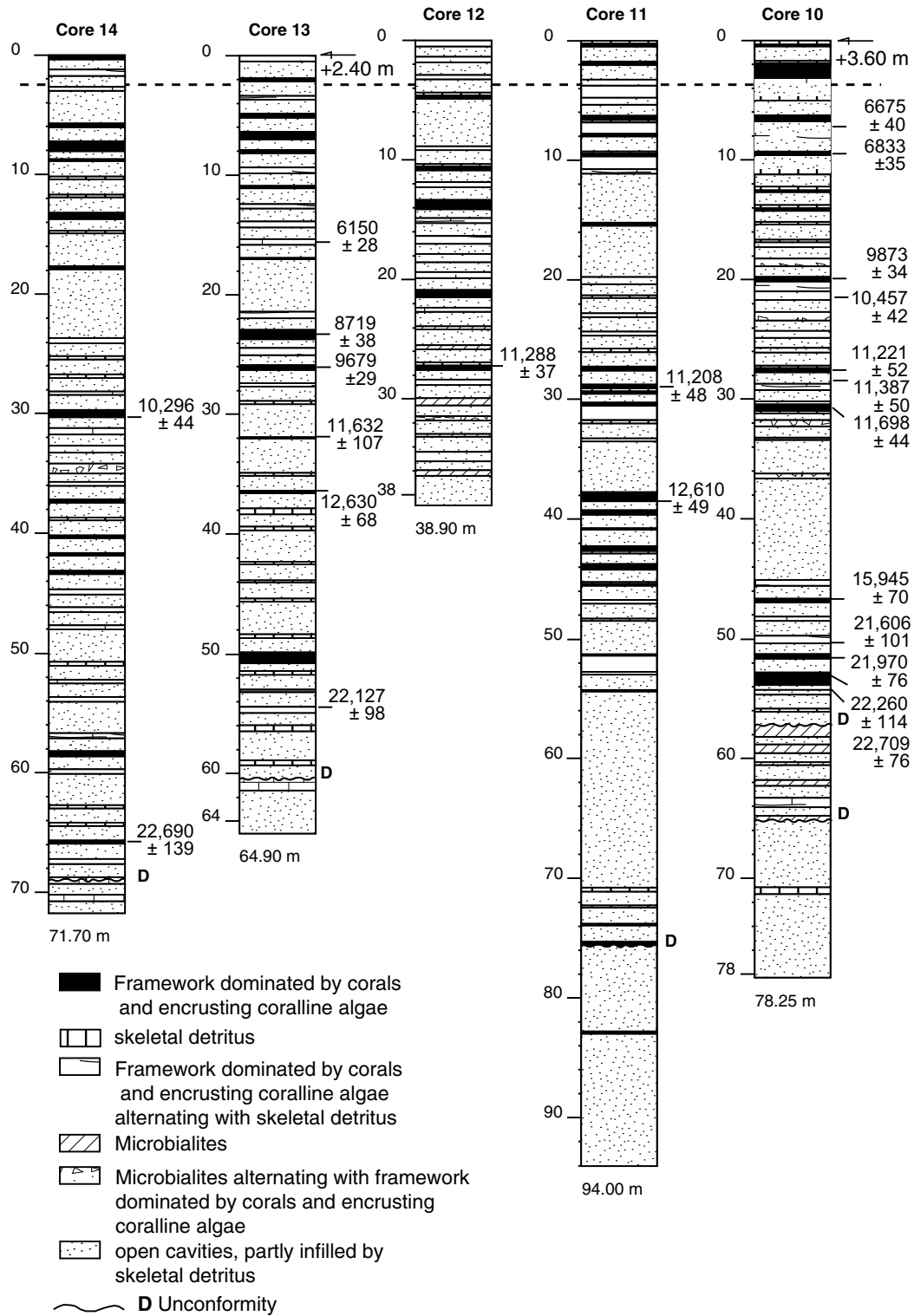


Figure 17 Vanuatu core logs 10-14

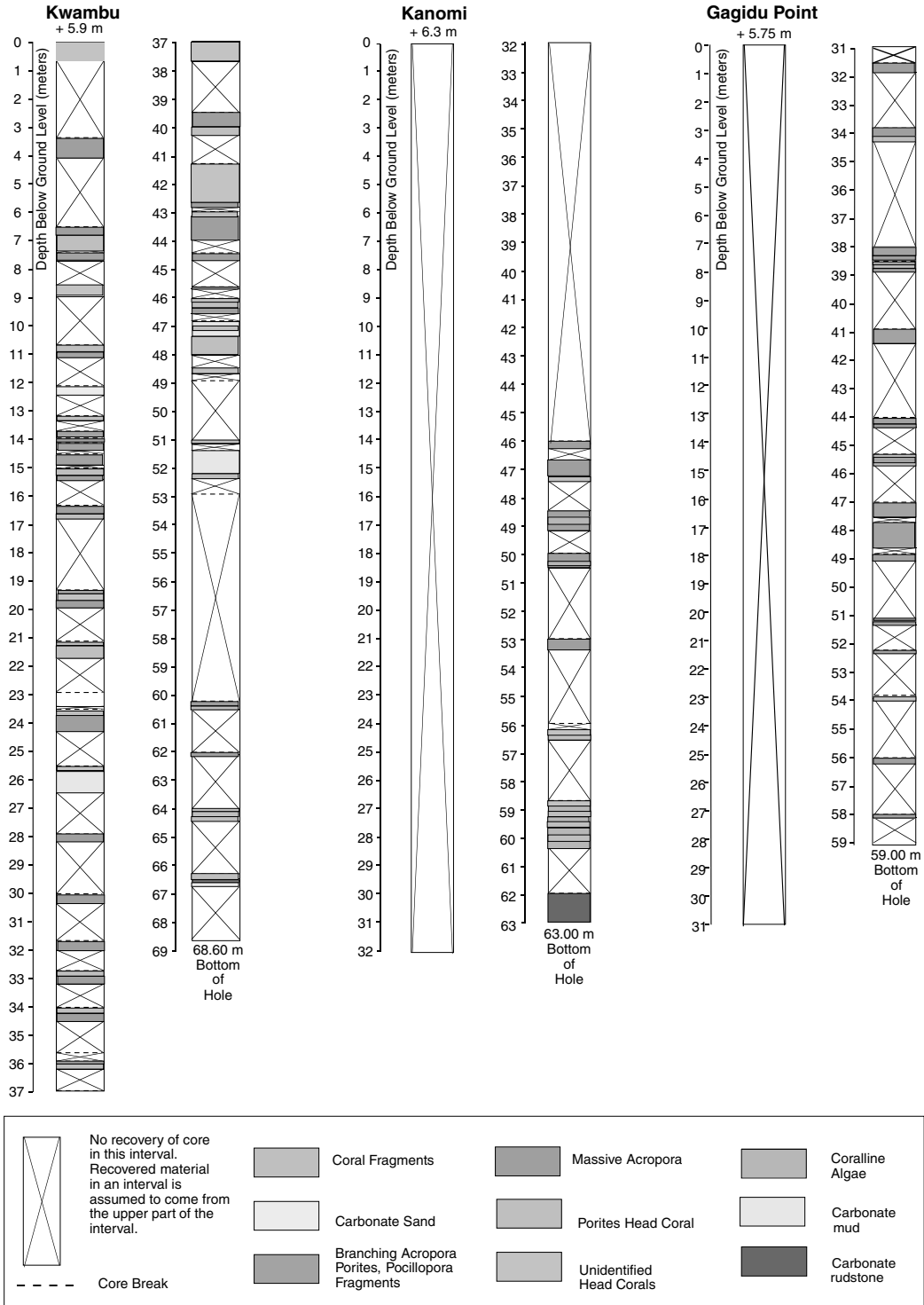


Figure 18 Papua New Guinea core logs